Hypoxia-driven heterogeneous expression of α5 integrin in glioblastoma stem cells is linked to HIF-2α

Mélissa Messé, Chloé Bernhard, Sophie Foppolo, Lionel Thomas, Patrice Marchand, Christel Herold-Mende, Ahmed Idbaih, Horst Kessler, Nelly Etienne-Selloum, Charles Ochoa, et al.

BBA - Molecular Basis of Disease 1870 (2024) 167471

Contents lists available at ScienceDirect

BBA - Molecular Basis of Disease

journal homepage: www.elsevier.com/locate/bbadis

Hypoxia-driven heterogeneous expression of α5 integrin in glioblastoma stem cells is linked to HIF-2α

Mélissa Messé [a,b], Chloé Bernhard [a], Sophie Foppolo [a], Lionel Thomas [b], Patrice Marchand [b], Christel Herold-Mende [c], Ahmed Idbaih [d], Horst Kessler [e], Nelly Etienne-Selloum [a,f], Charles Ochoa [g], Uttam K. Tambar [g], Mohamed Elati [h], Patrice Laquerriere [b], Natacha Entz-Werle [a,i], Sophie Martin [a], Damien Reita [a,j], Monique Dontenwill [a,*]

[a] UMR7021 CNRS, Tumoral Signaling and Therapeutic Targets, Strasbourg University, Faculty of Pharmacy, Illkirch, France
[b] UMR7178 CNRS, Hubert Curien Multidisciplinary Institute, Strasbourg University, 67000 Strasbourg, France
[c] Division of Neurosurgical Research, Department of Neurosurgery, Heidelberg University Hospital, 69120 Heidelberg, Germany
[d] Sorbonne University, AP-HP, Institut du Cerveau - Paris Brain Institute - ICM, Inserm, CNRS, Hôpitaux Universitaires La Pitié Salpêtrière - Charles Foix, F-75013 Paris, France
[e] Institute for Advanced Study, Department Chemie, Technical University Munich (TUM), Lichtenbergstr. 4, 85747 Garching, Germany
[f] Pharmacy department, Institut de Cancérologie Strasbourg Europe (ICANS), 67200 Strasbourg, France
[g] Department of Biochemistry, The University of Texas Southwestern Medical Center at Dallas, 5323 Harry Hines Boulevard, Dallas, TX 75390-9038, United States
[h] Univ. Lille, CNRS, Inserm, CHU Lille, UMR9020-U1277 – CANTHER – Cancer Heterogeneity Plasticity and Resistance to Therapies, Lille F-59000, France
[i] Pédiatrie Onco-Hématologie-Pédiatrie III, Strasbourg University Hospital, 67091 Strasbourg, France.
[j] Department of Cancer Molecular Genetics, Laboratory of Biochemistry and Molecular Biology, University Hospital of Strasbourg, 67200 Strasbourg, France

ARTICLE INFO

Keywords:
Glioma stem cells
Hypoxia
α5 integrin
HIF-2α

ABSTRACT

Despite numerous molecular targeted therapies tested in glioblastoma (GBM), no significant progress in patient survival has been achieved in the last 20 years in the overall population of GBM patients except with TTfield setup associated with the standard of care chemoradiotherapy. Therapy resistance is associated with target expression heterogeneity and plasticity between tumors and in tumor niches. We focused on α5 integrin implicated in aggressive GBM in preclinical and clinical samples. To address the characteristics of α5 integrin heterogeneity we started with patient data indicating that elevated levels of its mRNA are related to hypoxia pathways. We turned on glioma stem cells which are considered at the apex of tumor formation and recurrence but also as they localize in hypoxic niches. We demonstrated that α5 integrin expression is stem cell line dependent and is modulated positively by hypoxia *in vitro*. Importantly, heterogeneity of expression is conserved in *in vivo* stem cell-derived mice xenografts. In hypoxic niches, HIF-2α is preferentially implicated in α5 integrin expression which confers migratory capacity to GBM stem cells. Hence combining HIF-2α and α5 integrin inhibitors resulted in proliferation and migration impairment of α5 integrin expressing cells. Stabilization of HIF-2α is however not sufficient to control integrin α5 expression. Our results show that AHR (aryl hydrocarbon receptor) expression is inversely related to HIF-2α and α5 integrin expressions suggesting a functional competition between the two transcription factors. Collectively, data confirm the high heterogeneity of a GBM therapeutic target, its induction in hypoxic niches by HIF-2α and suggest a new way to attack molecularly defined GBM stem cells.

1. Introduction

Since 2005, the glioblastoma standard of care consists of surgery (when possible) followed by chemoradiotherapy with Temozolomide named the Stupp protocol [1]. The most important advance in 20 years has been the use of TTfields in conjunction with the standard protocol [2]. Despite numerous preclinical positive results with targeted therapies, clinical trials failed to improve patient overall survival. Although clinically characterized by common histological features, accumulating data report that glioblastoma (GBM), the most aggressive brain tumors,

* Corresponding author at: UMR 7021 CNRS, LBP, Strasbourg University, Faculty of Pharmacy, 67401 Illkirch, France.
E-mail address: monique.dontenwill@unistra.fr (M. Dontenwill).

https://doi.org/10.1016/j.bbadis.2024.167471
Received 21 November 2023; Received in revised form 27 July 2024; Accepted 12 August 2024
Available online 21 August 2024

correspond to a family of molecularly distinct entities. Integrated genomic, transcriptomic, epigenomic and proteomic analysis allowed the definition of core biological pathways and clinically relevant subtypes of GBM [3–6]. A robust gene expression-based molecular classification of GBM into four subgroups (proneural, neural, classical and mesenchymal) has been proposed in 2010 by the Cancer Genome Atlas Network [7] but neural subclass was since assigned to non tumoral cells [8]. Other layers of complexity have been characterized including the GBM stem cell (GSC) subsets and their high plasticity [9–13]. As these stem-like cells are considered to initiate brain tumors upon orthotopic implantation, to sustain tumor growth, and to escape chemo-radiotherapy-induced cell death [14], it is essential to understand their biology. Tumor cells with stem-like properties are classically cultured from GBM tumor bulk biopsies by using conditions selecting for neural stem cells. They are able to form neurospheres *in vitro* that recapitulate the histopathology of human GBM tumors when xenotransplanted in nude mice, such as pseudopalisading necrosis, nuclear pleomorphism and extensive microvascular proliferation [15]. They also maintain the clonal and genomic complexity of the parental patient tumors [11,16,17].

Integrins are involved in most hallmarks of cancer [18,19] and their implications in brain tumor aggressiveness have been highlighted [20]. Some data exist on integrins in brain cancer stem cells [21]. Among them, the α6 integrin (ITGA6 receptor for laminin) enriches for GSC and has been involved in their self-renewal, proliferation and tumor formation capacity [22]. The α6 integrin mRNA level also negatively correlates with glioma patient survival in the REMBRANDT database [23]. Similarly, α3 integrin (ITGA3) was proposed to be overexpressed in GSC and to promote invasion [24]. More recently, α7 integrin (ITGA7) was shown to be specifically expressed in GSC compared to differentiated cells and to be a marker for aggressive and invasive tumors [25]. Finally, β8 integrin (ITGB8) similarly appeared as a marker of GSC involved in tumor initiation, progression and resistance to radiotherapy [26,27]. We [28] and others [23,29] have shown that patient bulk tumors express varying levels of α5 integrin (ITGA5) mRNA, negatively correlated with glioma patient survival. Our recent data confirm that ITGA5 protein expression is effectively correlated to Stupp protocol treatment resistance [30]. No data currently support its potential role in GSC as a biomarker of aggressiveness. Starting from patient transcriptomic data (TCGA data), we show by GSEA analysis that overexpression of ITGA5 was linked to different pathways including hypoxia. We therefore investigated the expression of ITGA5 protein in GSC maintained in stem cell medium either in normoxia or in hypoxia as it is already known that GSC localize in hypoxic niches. In contrast with data on other integrins, we found that only a subpopulation of GSC is programmed to express it in normoxia and that hypoxic conditions rather increase this expression in a timely manner *in vitro*. ITGA5 –expressing GSC keep this property *in vivo* leading to more aggressive and invasive tumors. We demonstrated that among hypoxia-induced factors, HIF-2α predominantly modulated the expression of ITGA5. This HIF-2α-driven integrin expression confers enhanced migration potency to GSC. Even if ITGA5 appeared not to be involved in GSC proliferation, combining HIF-2α inhibitors with ITGA5 specific antagonist resulted in a clear proliferation inhibition of selected GSC. Specific HIF-2α inhibitors in addition with integrin antagonists thus represent new therapeutic options to treat ITGA5 expressing GBM. Lastly, our results support the hypothesis of an inverse relationships between HIF-2α and AHR for ITGA5 induction opening the way to new investigations on how to consider molecular heterogeneity of therapeutic targets in GBM.

2. Materials and methods

2.1. Gene set enrichment analysis

To explore signaling pathways enrichment, Gene Set Enrichment Analysis (GSEA) [31] was performed between low and high ITGA5 expression groups using GSEA Java software (https://www.gsea-msigdb.org/gsea/index.jsp version 4.2.3) with MSigDb Hallmark gene sets [32]. Expression data were obtained from the Affymetrix HT HG U133A array of TCGA GBM dataset. This dataset consists of tumor samples from 538 patients with newly diagnosed glioblastoma prior treatment. GBM samples were divided according to the median expression of ITGA5 gene into high and low expression groups. Only results from high ITGA5 expression groups are shown.

2.2. Cell lines and cell culture conditions for GSC

Six different patient-derived GBM stem cell lines were used. NCH644 and NCH421k glioma stem cells were provided by Dr. Herold-Mende (Department of Neurosurgery, University of Heidelberg, Germany). Glioma stem cells 3731 and 5706 were provided by Dr. Idbaih (Paris Brain Institute, ICM, Paris). TC7 and TC22 glioma stem cells were obtained from patient-derived heterotopic xenografts (PDX) in the Laboratory of Bioimaging and Pathology (UMR7021 CNRS, Illkirch). Cells were cultured in Dulbecco's Modified Eagle medium with nutrient Mixture F-12 and GlutaMAX™ (DMEMF12 + GlutaMAX™, Gibco™), supplemented with 20 % of BSA Insulin Transferrin (BIT-100, Provitro), 20 ng/mL of EGF and 20 ng/mL β-FGF (Reliatech). All cell lines were maintained in a 37 °C incubator, with 5 % CO_2. Neurospheres were dissociated every 7 days with accutase (A6964, Sigma) and then put back into culture. For the hypoxic condition, cells were cultured in a trigas incubator in which oxygen levels were reduced to 1 % by nitrogen injection. For specific treatments, cells were incubated with drugs detailed in Table 2.

2.3. Western Blot analysis

Cells were directly lysed with 2× Laemmli Sample Buffer (60 mM Tris-HCl pH 6.8; 20 % glycerol; 2 % SDS; 0.01 % bromophenol blue - Biorad) supplemented with 5 % β-mercaptoethanol (Biorad) on ice and denatured at 95 °C for 13 min. Lysates were electrophoresed using 4–20 % SDS-PAGE polyacrylamide gels (Biorad) and then transferred to a PVDF membrane (GE Healthcare, Velizy, France). PVDF membranes were blocked in 0.1 % Tween-20 Tris buffered saline (TBST) containing 5 % milk for 1 h at room temperature and incubated overnight at 4 °C with the corresponding primary antibody. Membranes were washed with TBST and incubated for 1 h at room temperature. With horseradish peroxidase (HRP)-conjugated secondary antibodies. After washing, blots were visualized using the enhanced chemiluminescence (ECL) system (ECL™ Prime Western Blotting System, GE Healthcare Bioscience) with an ImageQuant™ LAS 4000 analyzer (GE Healthcare). Quantification of unsaturated images was performed using ImageJ software (National institutes of Health, Bethesda, MD, USA, https://imagej.nih.gov). For each experiment, 3 lysates from different cell cultures were used. Tubulin was used as a loading control for all samples. List of antibodies is provided in Table 1.

2.4. RT-qPCR analysis

Cells were plated in a 6-well plate at a density of 1×10^6 cells/well in medium alone or in the presence of 20 μM PT2977 or 20 μM compound 2 for 24 h in 1 % O_2 hypoxia. After 24 h incubation, cells were washed with 1× PBS and the RNA extraction step was performed using the RNeasy Plus Mini Kit according to the manufacturer's instructions (Quiagen). RNA concentration was assessed using a NanoDrop™One UV–Visible spectrophotometer (ThermoFisher). Reverse transcription was performed using the "iScript™ Reverse Transcription Supermix" kit according to the manufacturer's instructions (Biorad) with a thermocycler (T100, Biorad). For RT-qPCR, a reaction mixture was made for each primer (Table 3) using SYBR Green™ as reagent, and 15 μL is poured into a MicroAmp™ 96-well optical reaction plate (Applied Biosystems™). The cDNA obtained by reverse transcription is diluted 5-fold

Table 1
List of antibodies used during the different experiments.

Antibodies list			
Label	Reference	Species	Dilution
ITGA5	Cell signaling (D7B7G)	Rabbit	1/1000 (WB)
ITGA5	BDBioscience IIaI (555,614)	Mousse	1/100 (FACS/ IF)
ITGA5	Millipore (AB1928)	Rabbit	1/500 (IF brain)
HIF-1α	Abcam (ab51608)	Rabbit	1/1000 (WB)
HIF-2α	Novus (Nb100-122)	Rabbit	1/1000 (WB)
CA9	Abcam (ab15086)	Rabbit	1/1000 (WB)
α-Tubulin	Sigma-Aldrich (T9026)	Mousse	1/1000 (WB)
Cadhérine	Proteintech (20874-1-20ul)	Rabbit	1/5000 (WB)
Vimentine	Proteintech (60330)	Mousse	1/5000 (WB)
Histone	Cell signaling (2595)	Rabbit	1/1000 (WB)
AhR	Cell signaling (D5S6H)	Rabbit	1/1000 (WB) 1/100 (IF)
Anti-rabbit IgG-HRP	Promega (W4018)	Goat	1/10000 (WB)
Anti-mousse IgG-HRP	Promega (W4028)	Goat	1/10000 (WB)
Alexa fluor™ 568 rabbit IgG	Invitrogen (A11011)	Goat	1/500 (IF)
Alexa fluor™ 650 mousse IgG	Invitrogen (SA5-10174)	Goat	1/500 (IF)

Table 2
List of drugs used during the different experiments.

Drugs list	
Label	Reference
Irinotecan	MedChemExpress (HY-16562)
PT2977	MedChemExpress (HY-125840)
Compound 2	Dr. Tambar UK., Dallas [39]
FR248	Dr. Kessler H., Munich [43]
Compound 12a	MedChemExpress (HY-144339)

and 5 μL of DNA is added to this mixture in the 96-well plate. RT-qPCR is performed with the StepOnePlus™ real-time PCR instrument (4,376,357, Thermofisher) and run with StepOne™ software (v2.3). Data are then analyzed using this software. RNA18S is used as an endogenous control. List of primers is provided in Table 3.

2.5. Transfection of siRNA

Cells were seeded at a density of 500,000 cells/well in a 6-well plate previously coated with 20 μg/mL Cell-Tak™ (Corning). The cells were then transfected with the corresponding siRNA (Qiagen) at 100 nM for HIF-1α, 250 nM for HIF-2α or 50 nM for ITGA5 according to the following steps. A solution of siRNA at the appropriate concentration was prepared in 250 μL Opti-MEM, together with a solution of 5 μL of Lipofectamine 2000 (ThermoFisher) in 250 μL Opti-MEM. These 2 solutions were incubated at room temperature for 5 min before being mixed together. This mix was incubated at room temperature for 25 min before being added to the cells in the culture medium. For experiments with HIFs repression, cells were placed in 1 % O_2 hypoxia for 48 h. For experiments with ITGA5 repression, cells were subjected to sphere evasion assay protocol. For all experiments protein expression was checked by western blot analysis.

2.6. Proliferation assays (Incucyte®)

3000 stem cells/well were plated in a 96-well plate in the medium alone or with different treatments. Cells were then placed in a trigaz incubator containing the Incucyte equipment for 6 days at 37 °C, 5 % CO_2 in normoxia (20 % O_2) or hypoxia (1 % O_2). Neurosphere size (μm^2) was monitored using an IncuCyte™ Zoom live cell analysis system. The IncuCyte® technology took images every 4 h and neurosphere size was recorded for each time point and normalized to time zero.

2.7. Sphere evasion assays

Neurospheres were generated using the suspended drop method to get homogenous population of spheres [70]. A cell suspension of 2000 cells/20 μL of growth medium supplemented with 1.2 % methylcellulose (Sigma Aldrich, M0262) was deposited on the inner surface of a Petri dish. After 48 h, each spheroid was transferred to a 24-well plate coated with poly-L-lysine (Sigma Aldrich, P8920) or fibronectin (Promocell, C-43060) (1 sphere per well) with medium alone or with treatments of interest. Cells were then placed in normoxia at 20 % O_2 or hypoxia at 1 % O_2 in a trigz incubator. Invasion was monitored for 24 h, then spheroids were fixed with 1 % (vol/vol) glutaraldehyde (Thermo Fisher Scientific, 16,400) for 30 min, followed by DAPI staining (Sigma Aldrich, D9542) at 1 μg/mL for 45 min. An epifluorescence microscope was used to take photos. The number of migrating cells was determined with ImageJ software using an in house developed macro.

2.8. Immunocytofluorescence

Cells were seeded on coverslips previously coated with poly-L-lysine (10 μg/mL) and placed in a 24 well plate. After incubation in normoxia or hypoxia for 72 h, cells were fixed in cold methanol for 10 min on ice. After a permeabilization step in PBS 1×, 0.2 % Tween20 for 15 min and a blocking step in PBS 1×, 5 % normal goat serum, 3 % BSA for 1 h at room temperature, cells were incubated with primary antibodies (Table 1) overnight at 4 °C. After washing with PBS, cells were incubated for 1 h at room temperature with the corresponding secondary antibodies and DAPI (10 mg/mL, Sigma-Aldrich). The coverslips were mounted with FluoreGuard mounting medium (ScyTek). Images were acquired using a Leica TCS SPEII confocal microscope (Leica microsystems SA) with a 63× magnification oil immersion objective and analyzed with ImageJ software. All confocal microscope settings were kept constant between each immunostaining experiment.

2.9. Orthotopic xenograft

Eight-week-old female NUDE NMRI mice were obtained from Janvier labs. CSG lines TC22 (α5+) and NCH421k (α5-) were dissociated and injected at a density of 25,000 cells in 2 μL of culture medium into the left striatum of the mouse. Each cell line was injected into a group of 5 mice. Mice were placed in a stereotaxic frame after being anesthetized in an induction chamber with 2.5 % isoflurane. A mask was placed over the muzzle of the mice to maintain anesthesia with 2.5 % isoflurane. The coordinates used for cell injection were as follows: X = − 0.5; Y = + 1.5; Z = − 3 mm from the bregma. A Hamilton syringe was used to inject stem cells at a rate of 1 μL/min. At the onset of neurological symptoms and/or weight loss (20 % of mouse weight), after anesthesia, mice were

Table 3
List of primers used during the different experiments.

Primers list			
Label	Reference	Primer sequence Forward	Primer sequence Reverse
ITGA5	Invitrogen	5'-TGCTGACTCCATTGGTTTCACAG-3'	5'-TCTCTCTGCAATCCTCTCGAGC-3'
RNA18S	Invitrogen	5'-TGTGGTGTTGAGGAAAGCAG-3'	5'-TCCAGACCATTGGCTAGGAC-3'

sacrificed with a euthanasia agent (Euthasol®). Experiments were performed in compliance with local laws and ethics committee approval (institutional protocol approval number 26600). Animal care was in accordance with institution guidelines.

2.10. Positron emission tomography (PET) imaging

Mice were evaluated by PET imaging from day 19 after stem cell injection, with weekly PET imaging sessions for 1 month. Two radiotracers were used: [^{18}F]-FLT ([^{18}F]-fluoro-thymidine) to assess cell proliferation and [^{18}F]-FET ([^{18}F]-fluoroethyl-L-tyrosine) to monitor tumor growth. Each radiotracer was produced by the CYRCE (Cyclotron for Research and Education) platform of the pluridisciplinary Hubert Curien Institute (IPHC, UMR 7178 CNRS, Strasbourg) using automated processes on AIO (Trasis®) module. Precursors and authentic references were purchased from ABX (Germany). Radiotracers were diluted in 0.9 % sterile NaCl (BBraun, veterinary grade) and injected intravenously into the tail vein. Each mouse was injected with an average of 10 MBq. Once biodistribution was complete ([^{18}F]-FLT = 90 min; [^{18}F]-FET = 45 min), the mice were anesthetized with 2.5 % isoflurane and placed in the PET/scan Inviscan® dedicated to small animals. A 10 min static acquisition was performed and the images were reconstructed using the iterative 3D ordered subset maximization algorithm (volume 201 × 201 × 120 mm^3). PET data were fully corrected for normalization, random coincidences, radioactive decay and dead time during the reconstruction process. No attenuation and scatter corrections were applied. Mice were maintained under anesthesia throughout image acquisition with 2.5 % isoflurane. Images were obtained using HOROS® software and tumor volume was calculated using Amide® software (http://amide.sourceforge.net/index.html). The tumor was delimited manually (ROI) then the SUVmax (Standardized Uptake Value maximum) was calculated by the software using the following formula:

$$SUV = (\text{Volume activity ROI}) \div ((\text{Injected activity}) \div (\text{Mouse weight}))$$

Tumor volume at 40 % of SUVmax was calculated to exclude experimental bias in tumor delineation.

2.11. Immunohistofluorescence

After sacrifice of the mice reaching the end points, the brains were recovered and fixed in 4 % paraformaldehyde overnight. The brains were then embedded in paraffin. Slices (5 μm thick) were deparaffinized, rehydrated and subjected to antigen unmasking protocol using Dako (Tris/EDTA) pH 9 recovery solution (Agilent Technologies, Les Ulis, France). After a blocking step in 1× PBS, 5 % normal goat serum, 0.1 % Tween-20 for 1 h at room temperature, sections were incubated with ITGA5 specific primary antibodies (Table 1) overnight at 4 °C. After washing in 1× PBS, 0.1 % Tween 20, tissue sections were incubated for 1 h at room temperature with the corresponding secondary antibodies and 1 μg/mL DAPI (Sigma-Aldrich). The coverslips were mounted using FluoreGuard mounting medium (ScyTek). Images were acquired on a Leica TCS SPEII confocal microscope with an oil immersion objective at 63× magnification. All confocal microscope settings were kept constant between each immunostaining experiment.

2.12. FACS analysis

A pellet of 100,000 dissociated cells was prepared. After 3 washes with PBS 1×, BSA 1 %, the cell pellets were resuspended and incubated for 30 min at 4 °C with the primary antibodies. The pellets were washed twice in PBS 1×, 1 % BSA, then resuspended and incubated for 30 min at 4 °C in the dark with the appropriate secondary antibodies. After 2 washes in PBS 1×, 1 % BSA cells were resuspended in 1× PBS and on a quant VYB MACS flow cytometer (Milteny). Results were analyzed using FCSalyzer software (0.9.22-alpha version, https://sourceforge.net/projects/fcsalyser).

2.13. Subcellular fractionation.

A pellet of 500,000 cells was prepared. Subcellular fractionation was performed with the Qproteome cell compartment kit (Qiagen) according to the manufacturer's instructions. The protein concentration was evaluated with a UV–Visible NanoDropTMOne spectrophotometer (Thermo Fisher). 10 μg of proteins from each fraction were lysed in 200 μL of 2× Laemmli (60 mM Tris-HCl pH 6.8; 20 % glycerol; 2 % SDS; 0.01 % bromophenol blue) (Biorad) supplemented with 5 % β-mercaptoethanol (Biorad) on ice and denatured at 95 °C for 13 min. Each compartment was checked by Western blot with specific antibodies.

2.14. Statistics

Data are expressed as mean ± SEM, and analyzed using GraphPad Prism version 5 (GraphPad Software, California, USA). Differences between groups were analyzed using a non-paired *t*-test and $p < 0.05$ was considered statistically significant.

3. Results

3.1. ITGA5 expression is linked to hypoxia and Epithelial to Mesenchymal Transition (EMT) in GBM patients

The subgrouping of GBM as high and low ITGA5 mRNA- or protein-expressing tumors already showed a clear impact of this integrin on patient survival [21,23,28–30]. We used publically available TCGA datasets to investigate the distribution of ITGA5 mRNA in the GBM molecular subtypes and confirmed that it was mainly associated with the mesenchymal subgroup already shown to be the most aggressive and resistant to therapies (Fig. 1A). Glioblastoma with a glioma-CpG island methylator phenotype (G-CIMP) express the least ITGA5 mRNA level although not achieving statistical significance compared to classical, proneural or neural glioma. Concerning intra-tumoral heterogeneity the IVY database pointed to an enrichment of ITGA5 mRNA expression in spatially defined regions of GBM, perinecrotic zones and perivascular zones (Fig. 1B). Gene set enrichment analysis (GSEA) was used to investigate the relationship of ITGA5 overexpression with biological processes in GBM. Transcriptomic data of 538 patients obtained from GBM cohort of TCGA were divided into 'high' and 'low' groups based on their ITGA5 expression according to the median expression of this gene. Using the Hallmark gene set, 5 pathways were highlighted in the 'high' group with TGF β signaling at the top which we already described in GBM as associated with ITGA5 [33]. Hypoxia (NES = 1.82, FDR q = 0.039) and EMT (EMT - NES = 1.76, FDR q = 0.031) were also highlighted in this analysis (Fig. 1C). Interestingly, the Hypoxia pathway appears specifically related to ITGA5/ITGB1 high expressing-tumors but not to ITGA7/ITGAV/ITGB3/ITGB4/ ITGB8/ITGA6 high-expressing tumors (Table 4). At the protein level, ITGA5 expression appeared heterogeneous between patients [30] but remarkably also in an intra-tumoral fashion (Fig. 1D). As perinecrotic and perivascular zones are proposed as GSC niches [34], we aimed to evaluate the putative expression of ITGA5 in these cells.

3.2. Heterogeneity of ITGA5 expression in GSC in vitro and in vivo

ITGA5 protein expression was evaluated in 6 stem cell lines. Few cell lines expressed it under normoxia conditions after neurosphere dissociation (Fig. 2A left). Interestingly, pseudo-hypoxic pathways are induced in neurospheres even if the microenvironment is normoxic, as shown by increased CA9, HIF-1α and HIF-2α expression, well-known hypoxia markers (Fig. 2A middle). Although CA9 and HIF-1α expression required the formation of neurospheres, HIF-2α is constitutively present in almost all lines, even in normoxia. These results confirm others as for example those obtained for neuroblastoma [35,36]. These markers appeared similarly expressed after 6 days under hypoxic

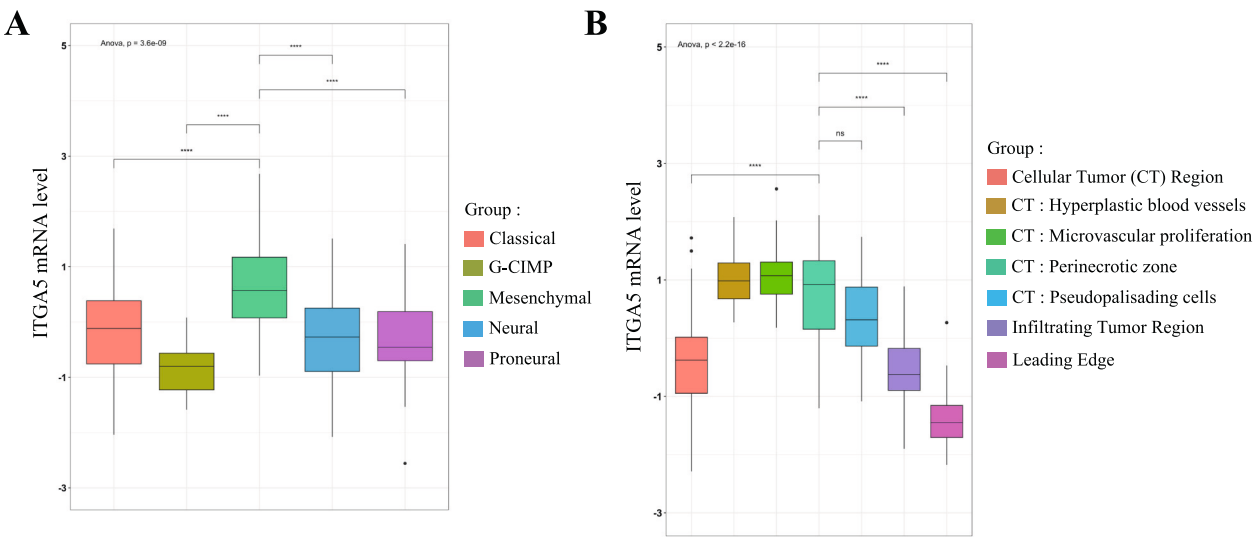

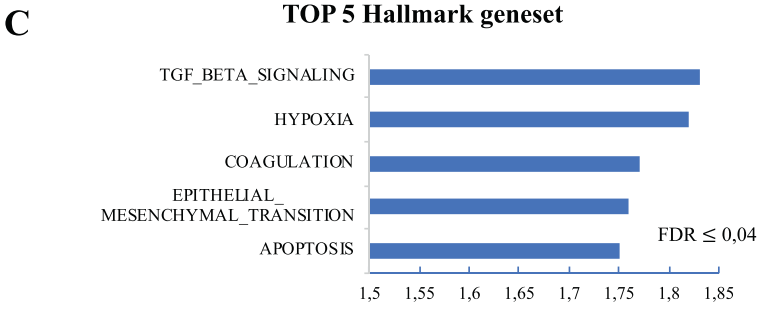

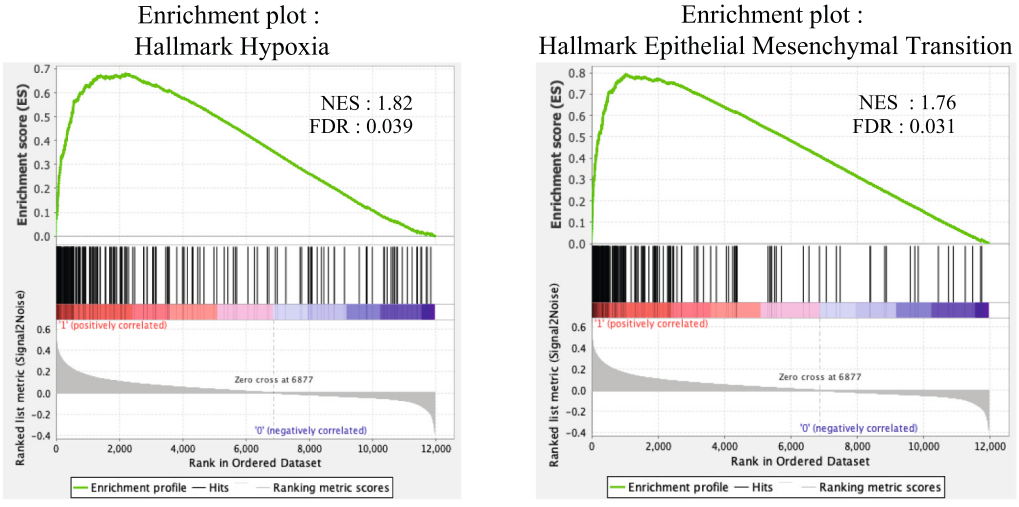

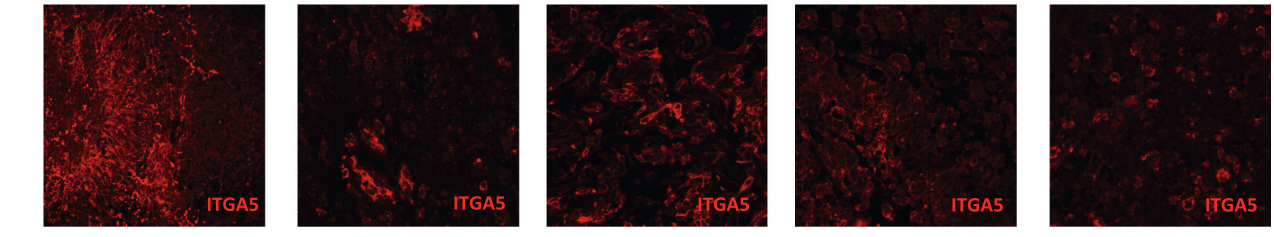

(caption on next page)

Fig. 1. Heterogeneity of ITGA5 expression and relationships to hypoxia and Epithelial to Mesenchymal transition in GBM patients.
A – expression of ITGA5 mRNA in GBM molecular subtypes (TCGA database). B – expression of ITGA5 mRNA in intra-tumor regions of GBM (IVY GAP data). C – Gene set enrichment analysis (GSEA) showing the 5 top enriched biological pathways in TCGA tumors with high level of ITGA5 mRNA. Enrichment plots for hallmarks Hypoxia and EMT gene sets. D –Heterogeneous immunostaining of ITGA5 protein in 5 different patient tumors.

conditions (Fig. 2A, right). In this case, ITGA5 expression increased significantly in the two already positive cell lines (3731 and TC22). Interestingly, we observe a strong expression of HIF-1α in ITGA5-negative lines compared to ITGA5-positive lines (Fig. 2A). HIF-2α overexpression compared to HIF-1α may be involved in ITGA5 expression. By cell immunofluorescence labeling with anti-ITGA5 antibodies, we confirmed the absence of ITGA5 expression in the 5706 cell line but expression in the TC22 cell line in normoxia. Interestingly, hypoxia increased ITGA5 in TC22 cells but in an heterogeneous manner with about 30 % of cells clearly highly positive (Fig. 2B). Similar results were obtained in 3731 cells (Fig. S1). Integrin expression occurs as expected mainly at the cell membrane as shown by FACS analysis and subcellular fractionation (Fig. S2A and B). ITGA5 and HIF2α/EPAS1 protein expression appeared related to their respective mRNA increase in hypoxia compared to normoxia for TC22 but not 5706 cells (Fig. S3).

GSC thus express differential levels of integrin α5 which can be exacerbated by hypoxia in specific cell lines. To confirm these *in vitro* data, we xenografted NCH421k and TC22 GSC lines (without or with ITGA5 *in vitro* expression respectively) into the brain of Nude mice. Brains were removed and labeled with Hematoxylin Eosin and specific anti-ITGA5 antibodies. As shown in Fig. 3A, NCH421k-derived tumors were small and devoid of ITGA5 labeling. By contrast, TC22-derived tumors were large and contained integrin-labeled tumor cells. GSC thus retained their capacity to express (or not) the integrin after *in vivo* implantation. We followed the growth behavior of the tumors by PET imaging using [^{18}F]-FLT, a marker of proliferation. Interestingly, TC22-derived tumors appeared more aggressive, rapidly growing and invading tumors (Fig. 3B) in relationships with poorer mice survival, (Fig. 3C) than NCH421k- derived tumors. Results were confirmed by another radiotracer [^{18}F]-FET (Fig. S4). Data suggest that molecular heterogeneity in GSC detected in *in vitro* conditions recapitulates the GSC-induced tumor heterogeneity for ITGA5 we already observed in patient tumors [30]. Although the TC22 tumor size and aggressiveness cannot be solely attributed to ITGA5 expression, both models may be useful to examine future therapeutic options including ITGA5 inhibitors.

3.3. Impact of HIF-1α and HIF-2α on ITGA5 expression

As hypoxia pathways appeared to be linked to expression of the integrin subunit (Figs. 1 and 2), we aimed to analyze more deeply these relationships. It is already known that the stability of HIFs is finely regulated by different oxygen levels. HIF-1α is expressed at lower levels of hypoxia compared to HIF-2α which is already present in normoxic conditions and more stable than HIF-1α [36,37]. Therefore, we evaluated the potential relationship between HIFs and ITGA5 expression at short time points (24, 48, and 72 h) (Fig. 4A). HIF-1α and HIF-2α behave differently in these conditions. HIF-1α increased up to 48 h of hypoxia before decreasing substantially at 72 h while HIF-2α increased gradually from 24 to 72 h for all cell lines. Interestingly, the temporal ITGA5 expression followed that of HIF-2α in the positive cell lines (3731 and TC22). It should also be noted that in both cell lines, HIF-2α reached a level 2.5 times higher (at 72 h) than that observed in normoxia, which is not the case for ITGA5 negative cells (NCH421k and NCH644) suggesting that an HIF-2α threshold may be involved in the sustained modulation of ITGA5 expression (Fig. 4A). Stabilization of HIFs may be obtained by chemical compounds such as cobalt chloride ($CoCl_2$) or desferrioxamine (DFO). Treatments with these compounds during 72 h also increased ITGA5 expression in the TC22 positive cell line but not in the NCH421k negative cell line corroborating the impact of HIFs in specific GSC lines (data not shown). Lastly, modulation of HIFs was checked in the TC22 cells cultured 3 days in hypoxia followed by 2 days in normoxia. Here again, HIF-1α appeared unstable and finely controlled with a rapid decrease in normoxic conditions in contrast to HIF-2α which remained expressed as was ITGA5 (Fig. S5).

Taken together, these results suggest a potential impact of HIF-2α on the expression of ITGA5 in GSC under hypoxia. We confirmed this hypothesis by linear regression analysis between HIF-1α or HIF-2α and ITGA5 expressions. HIF-2α and ITGA5 levels significantly correlated in TC22 and 3731 cell lines in hypoxic conditions in contrast to HIF-1α. (Fig. 4B). HIF-2α and ITGA5 expressions appeared thus linked in hypoxic conditions.

3.4. HIF-2α is preferentially linked to ITGA5 expression

We then aimed to clarify the role of HIF-1α and HIF-2α on ITGA5 expression in hypoxia. As a first attempt to selectively inhibit expression of HIF-1α, we used irinotecan, a topoisomerase 1 inhibitor, which was shown to alter the expression of HIF-1α by inhibiting its mRNA translation [38–40]. Integrin-positive TC22 cells were treated with 2.5 μM irinotecan for 72 h in 1 % O_2 hypoxia. In our GSC model, irinotecan not only inhibited HIF-1α but also HIF-2α expression associated with a disappearance of ITGA5 expression (Fig. 5A). Results were confirmed in 3731 cell line (Fig. S6A). To address more specifically the impact of each transcription factor, we used specific siRNA depletion. As shown in Fig. 5B, HIF-1α-siRNA specifically depleted their target gene but had no effect on ITGA5. Inversely, HIF-2α-siRNA decreased HIF-2α expression (20 %) and concomitantly ITGA5 by 30 % (Fig. 5B).

Finally, we checked specific HIF-2α inhibitors: PT2977 [41] and compound 2 [42]. These molecules recognize the PAS-B domain of HIF-2α and prevent its dimerization with the nuclear subunit HIF1-β also called ARNT thus inhibiting HIF-2α transcriptional activity. As PAS-B domain present a specific pocket on HIF-2α and these compounds bind to this pocket, they are highly specific for the inhibition of HIF-2α function [42,43]. Both compounds (20 μM) proved able to decrease ITGA5 mRNA after 24 h and ITGA5 protein after 72 h treatment in TC22 cells (Fig. 5C). Compound 2 also decreased HIF-2α expression perhaps explaining its better effect on ITGA5 (44 % decrease with compound 2 *versus* 19 % with PT2977) (Fig. 5C). In addition, colocalisation of HIF-2α and ITGA5 proteins were observed in specific area of TC22 xenografts (Fig. S7). Results suggest that HIF-2α is preferentially involved in the control of ITGA5 modulation particularly under hypoxia in GSC.

3.5. HIF-2α and ITGA5 as therapeutic targets in specific GSC

Based on our previous results, we hypothesized that hypoxia may affect phenotypically GSC in particular through ITGA5-dependent pathways. We already shown that this integrin is involved in migration and therapy resistance of differentiated GBM cells [18,44,45]. We now investigated if hypoxia-driven expression of the integrin may affect proliferation and/or migration of GSC. First, we assessed cell proliferation, with measure of neurosphere size as a readout, using Incucyte® technology. As shown in Fig. 6A, neurosphere size was not linked to enhanced expression of ITGA5. As for example TC22 (ITGA5+) and NCH644 (ITGA5-) cells have a larger sphere size after 6 days in normoxia compared to the other lines. Hypoxia only affected the neurosphere sizes of two cell lines, namely 3731 and NCH644 which respectively express or not the integrin as shown before (Fig. 6A). These data suggest that ITGA5 expression does not influence stem cell proliferation either in normoxia or in hypoxia.

As a confirmation, FR248, a specific antagonist of ITGA5, does not

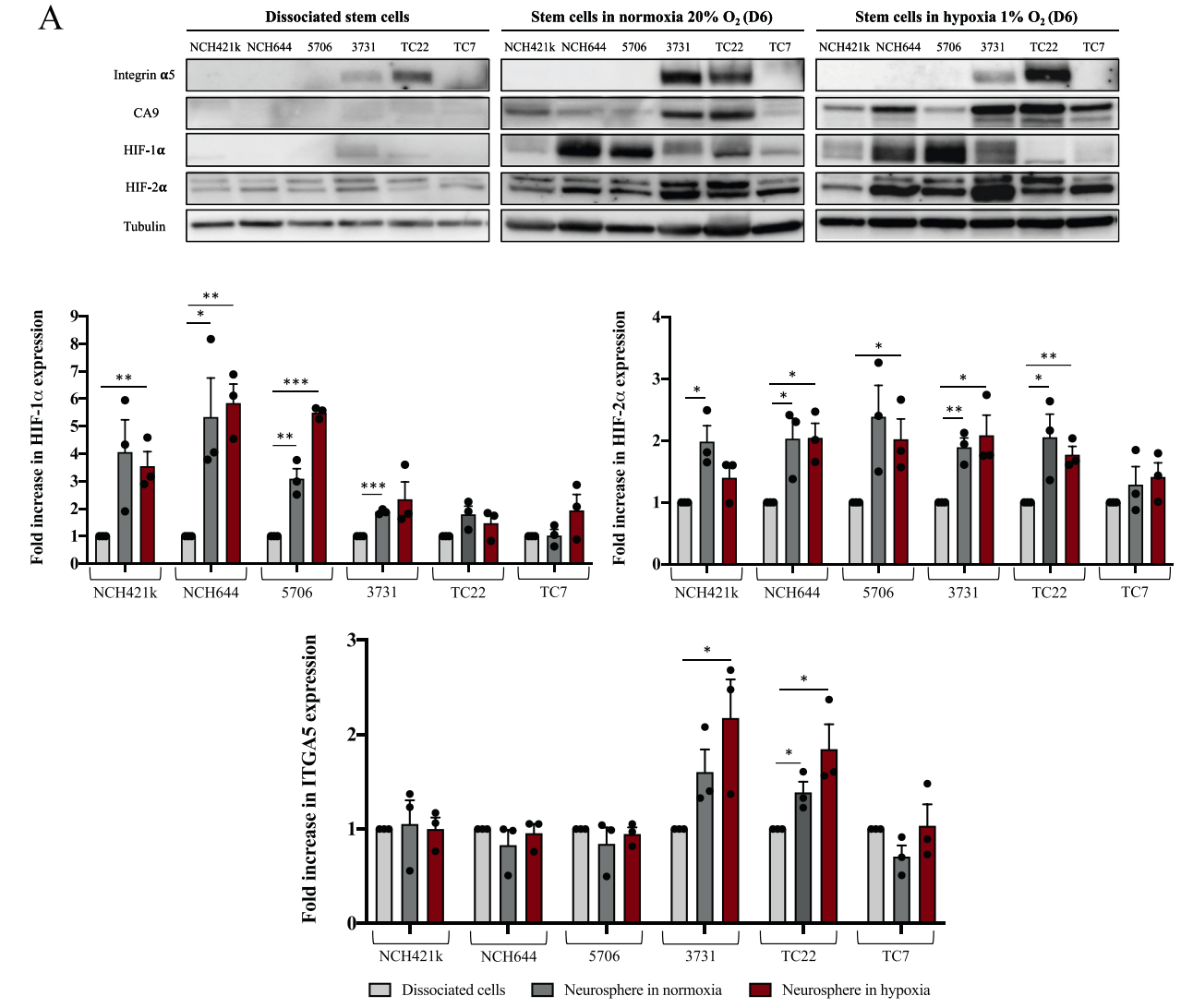

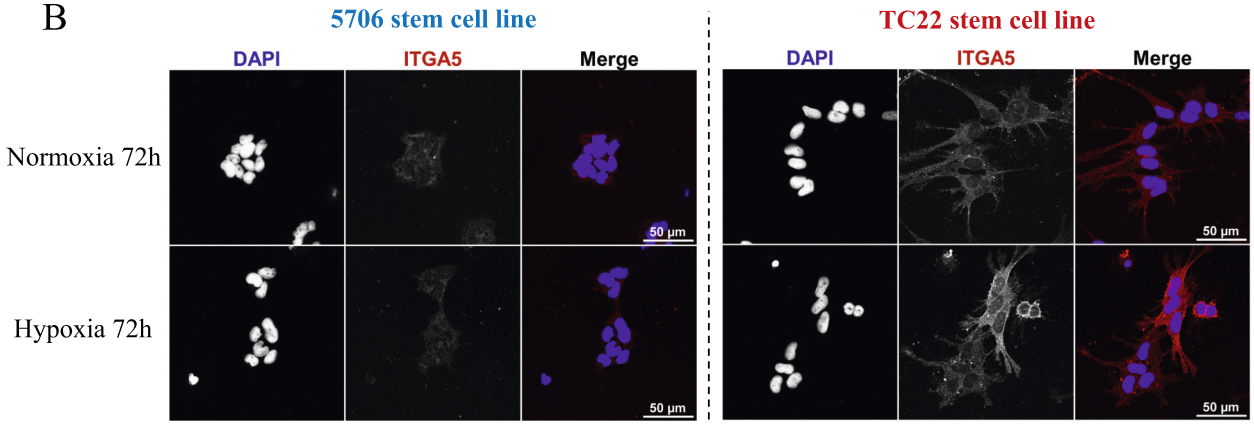

Fig. 2. Expression of ITGA5 protein in GBM stem cells under normoxia and hypoxia.
A - Western blot analysis of ITGA5 and hypoxia markers (HIF-1α, HIF-2α, CA9) in 6 GBM stem cell lines after 6 days in culture. Tubulin was used as a housekeeping protein. Histograms represent the mean ± S.E.M of 3 independent experiments. Different conditions are compared; dissociated neurospheres in normoxia (light grey bars), neurospheres in normoxia (dark grey bars) and neurospheres in hypoxia (red bars). *$p < 0.05$; **$p < 0.01$; ***$p < 0.005$. B - Immunofluorescent labeling of ITGA5 under normoxia (20 % O_2) and hypoxia (1 % O_2) in 5706 GSC and TC22 GSC.

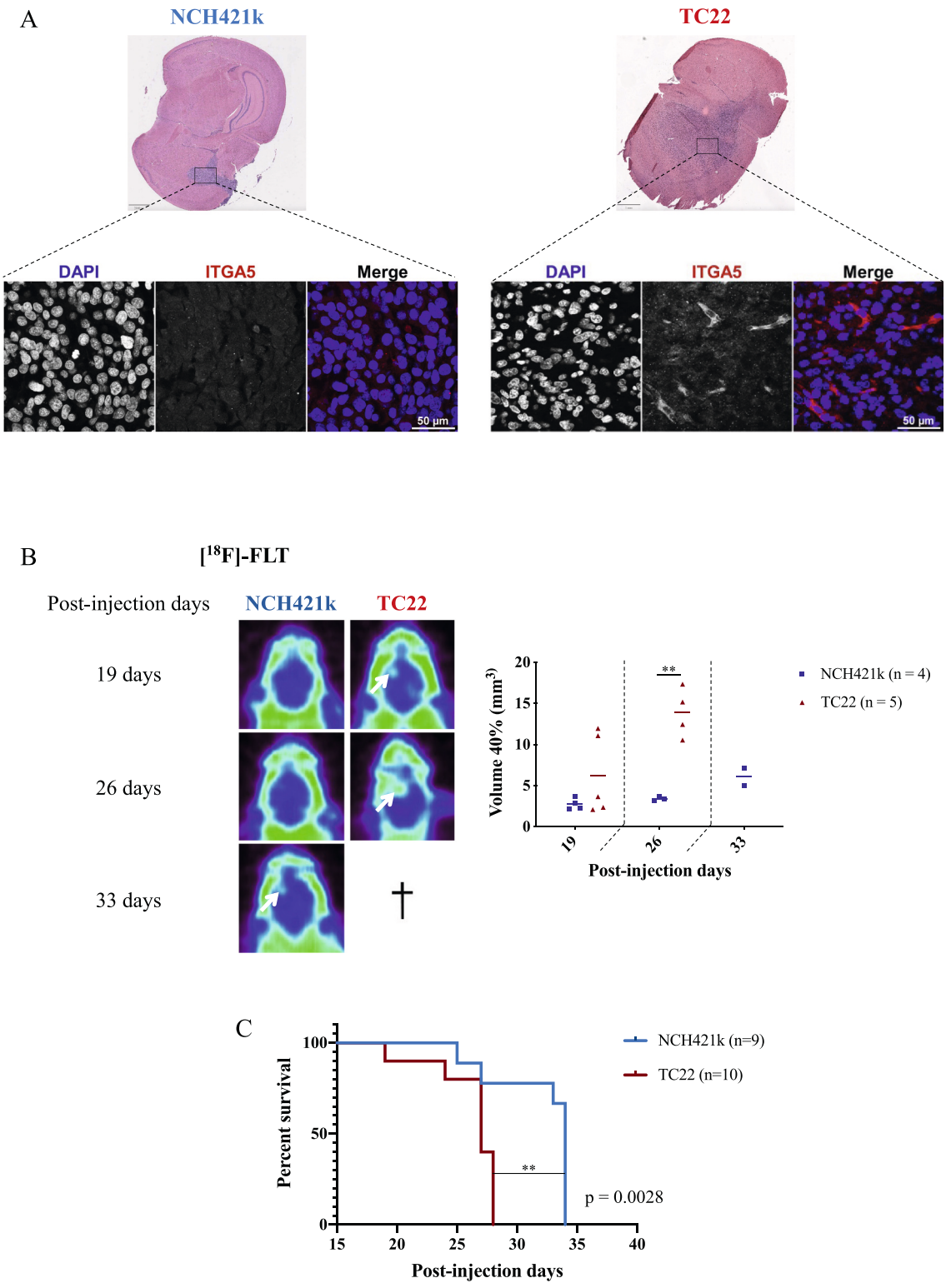

Fig. 3. Evaluation of GSC xenografts in Nude mice –relationships with ITGA5 expression.
A – Representative images of brain samples taken at the largest part of the tumor for TC22 and NCH421k GSC xenografts. Hematoxylin-eosin staining and ITGA5 immunofluorescence. B – PET monitoring of tumor growth with [^{18}F]-FLT. 2D frontal section images of mice and graphical representation of tumor volume quantification at 40 % Standardized Uptake Value (SUV) as a function of time post-injection. The white arrows indicate the tumors. C - Survival curve analysis from mice implanted intracranially with TC22 (n = 10 independent mice) and NCH421k cells (n = 9 independent mice). Survival analysis was performed using a Kaplan-Meier plot.

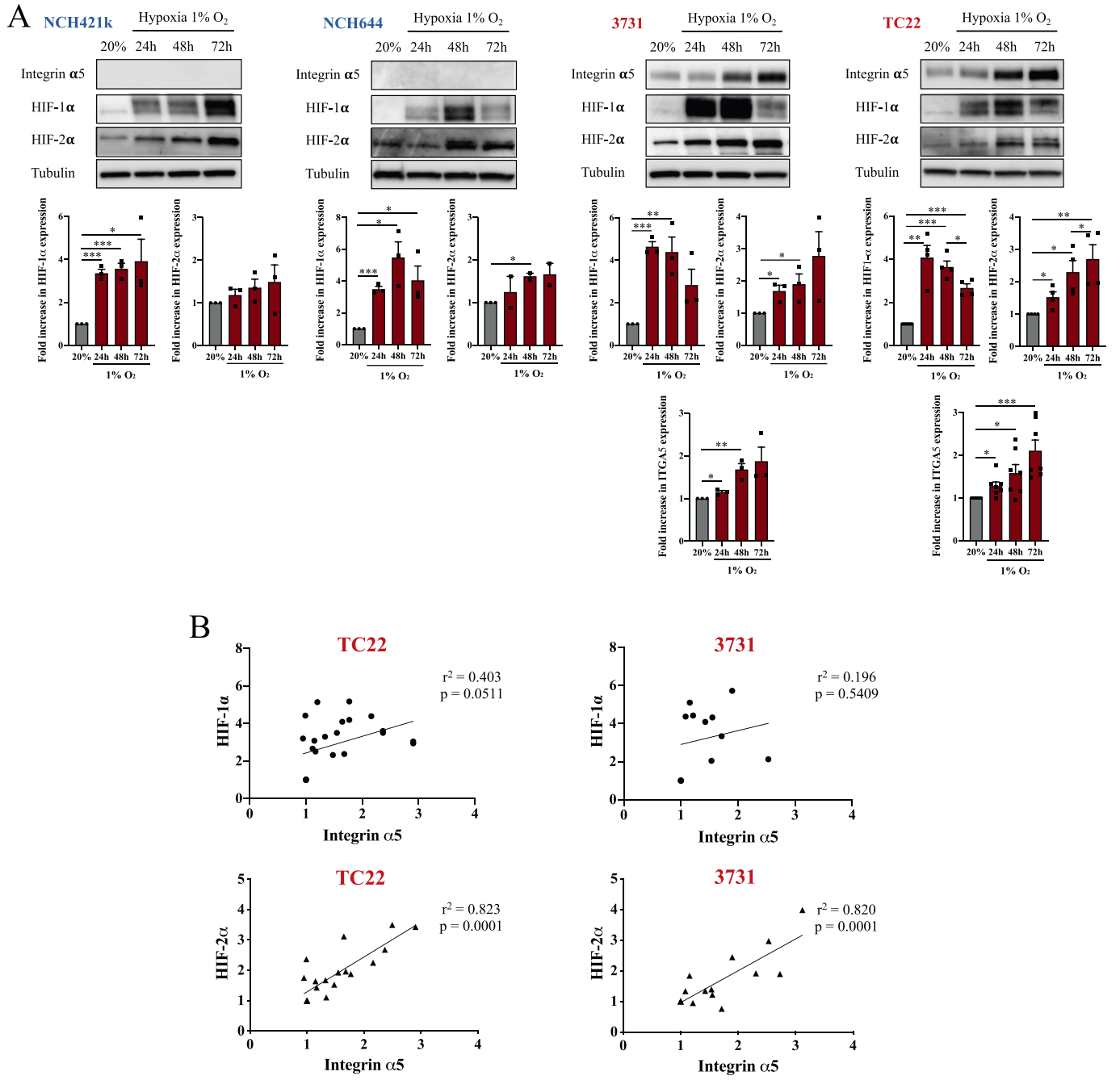

Fig. 4. Kinetics of HIF-1α, HIF-2α and ITGA5 expressions in GSC cells in normoxia and hypoxia.
A - Western blot analysis of ITGA5 and hypoxia-induced factors, HIF-1α and HIF-2α at 24, 48 and 72 h of GSC culture in normoxia (grey bars) and hypoxia (red bars). The relative quantification of each protein was performed according to the expression of tubulin. Histograms represent the mean ± S.E.M of 3 independent experiments with *p < 0.05; **p < 0.01; ***p < 0.005. B - Linear regression analysis of HIF-1α or HIF-2α *versus* ITGA5 expressions by Prism software.

alter neurosphere sizes either in integrin–expressing (TC22) or in non–-expressing cells (NCH421k) (Fig. 6B, light to dark orange bars). We then combined FR248 with compound 2 (20 μM) which is devoid of effect when used alone. Interestingly, the combination of FR248 (20 μM) and compound 2 (20 μM) decreased the neurosphere size in the ITGA5 positive line TC22 (58 % decrease) and 3731 (Fig.S6B) but not in the ITGA5 negative line NCH421k (Fig. 6B, light to dark blue bars). Data suggest that dual inhibition of HIF-2α and ITGA5 affects the proliferation of ITGA5-positive GSC thus providing a new therapeutic combination.

We then investigated the impact of hypoxia on stem cell migration. Spheres formed by the hanging drop technique, either with NCH421k or TC22 cells, were deposited on poly-L-lysine (neutral substrate for adhesion) or fibronectin (ECM ligand of ITGA5). On poly-L-lysine no cell evasion was detectable for both cell lines. By contrast, on fibronectin, cell evasion occurred for the TC22 line (ITGA5 positive) but not detectable for the NCH421k line (ITGA5 negative). Moreover, hypoxia increased this cell evasion by 30 % in the former line presumably in relation to the increased ITGA5 expression (Fig. 6C). To confirm this hypothesis, the spheres were treated with FR248 (20 μM) which inhibited completely the cell capacity to evade from spheres and to migrate on fibronectin either in normoxia or in hypoxia. Similar results were obtained when cells were treated with ITGA5 specific siRNA (Fig. S8). Data confirm the impact of this integrin on cell migration out of GSC spheres.

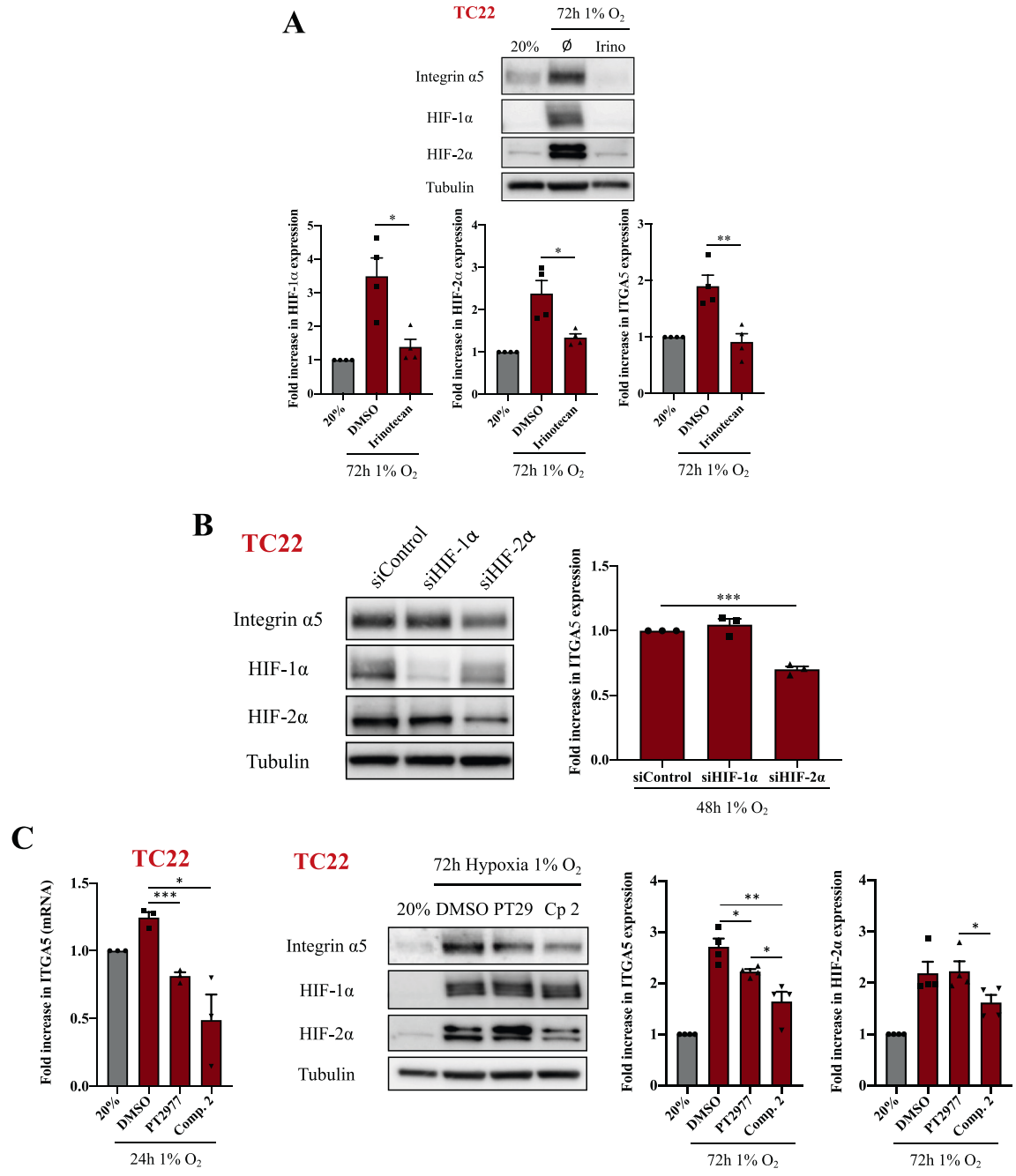

Fig. 5. Role of HIF-1α and HIF-2α for expression of ITGA5 in TC22 GSC in hypoxia.
A - Western blot analysis of irinotecan treatment on the expression of hypoxia-induced factors and ITGA5. TC22 stem cells were treated with 2,5 μM irinotecan for 72 h in 1 % O_2 hypoxia. The relative quantifications of each protein were performed according to the expression of tubulin. Histograms represent the mean ± S.E.M of 3 independent experiments with *p < 0.05; **p < 0.01; ***p < 0.005. Grey bars represent control conditions in normoxia and red bars neurospheres after 72 h in hypoxia. B - Western blot analysis of the impact of HIF-1α or HIF-2α siRNAs on ITGA5 expression. TC22 stem cells were treated with 100 nM HIF-1α siRNA or 250 nM HIF-2α siRNA for 48 h in 1 % O_2. Relative quantifications of protein expressions were performed according to the expression of tubulin. C - Analysis of the effect of treatments with specific HIF-2α antagonists on ITGA5 expression. Cells were treated with 20 μM PT2977 or 20 μM Compound 2 for 24 h (RT-qPCR analysis-left panel) or 72 h (WB analysis- middle and right panels) in 1 % O_2. Relative quantifications of the different expressions were performed based on the expression of RNA18S (RT-qPCR) or tubulin (WB). Histograms represent the mean ± S.E.M of 3 independent experiments with *p < 0.05; **p < 0.01; ***p < 0.005. Grey bars represent GSC in normoxia and red bars GSC in hypoxia.

As Compound 2 decreased ITGA5 expression by >40 % in TC22 cell line, we evaluated its effect on stem cell migration. Interestingly, compound 2 proved able to inhibit the cell evasion and migration in hypoxia suggesting here again the interconnection between HIF-2α and ITGA5. By contrast, PT2977 did not alter cell evasion (Fig. 6D) presumably linked to its weaker capacity to decrease both HIF2α and ITGA5 expressions in the TC22 line (see Fig. 5C).

Together, these results show for the first time that combining HIF2α and ITGA5 inhibition may be an alternative therapy for GSC. In addition, data show that stem cell migration on fibronectin is dependent on ITGA5 expression as was previously demonstrated on differentiated tumoral cells. This migration is enhanced by hypoxia and HIF-2α expression specifically. These data suggest that some GSC in hypoxic niches would acquire a migratory phenotype through modulation of the integrin expression.

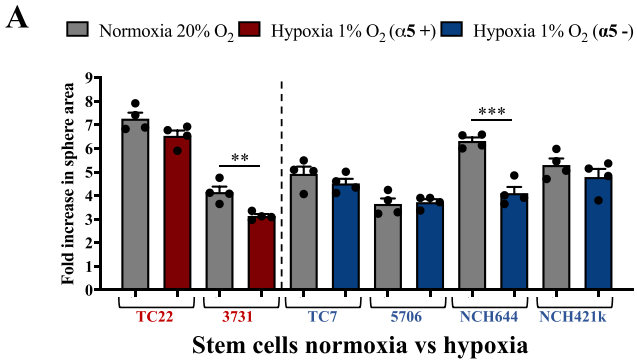

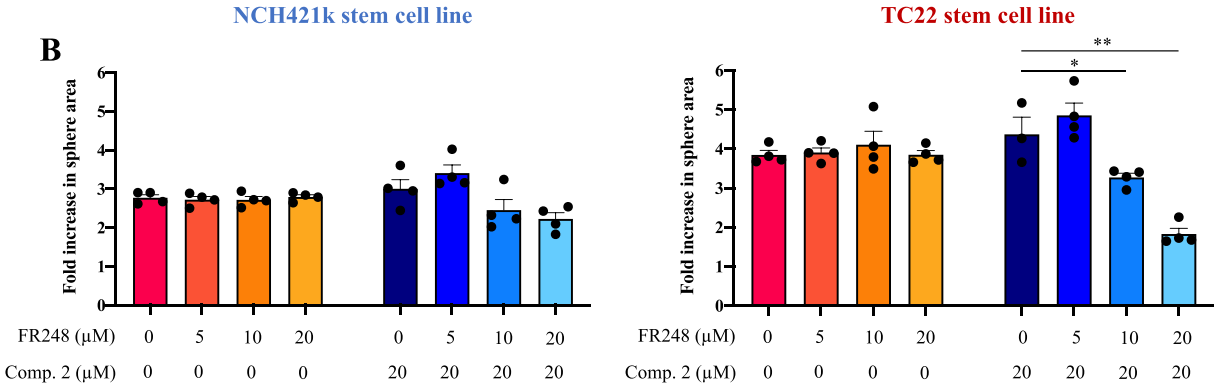

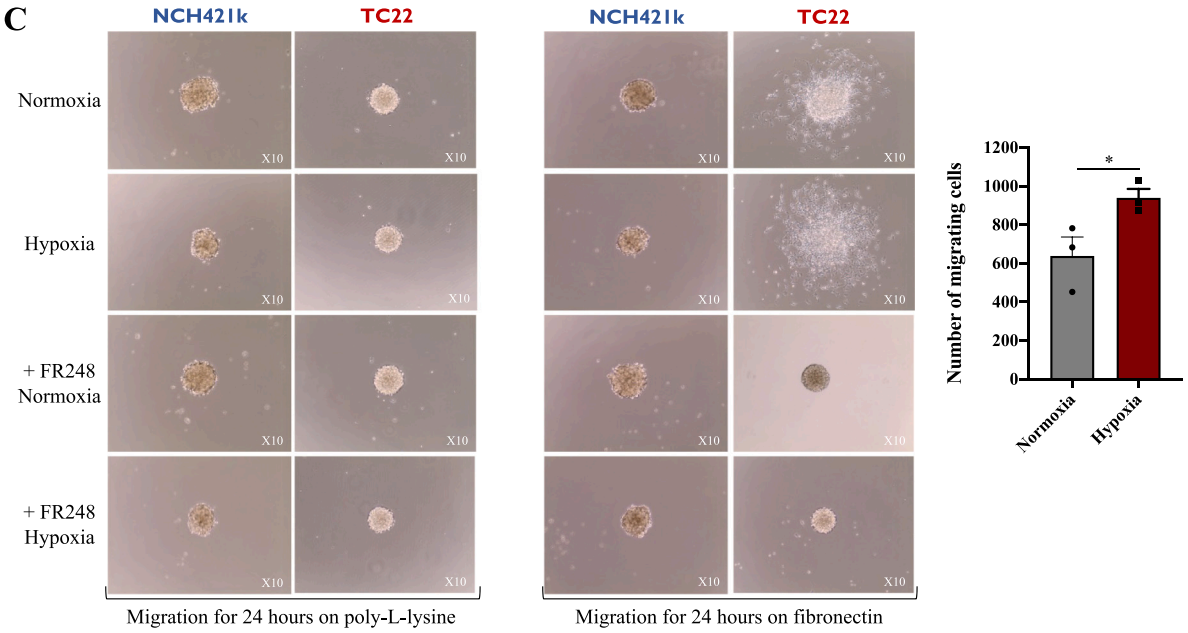

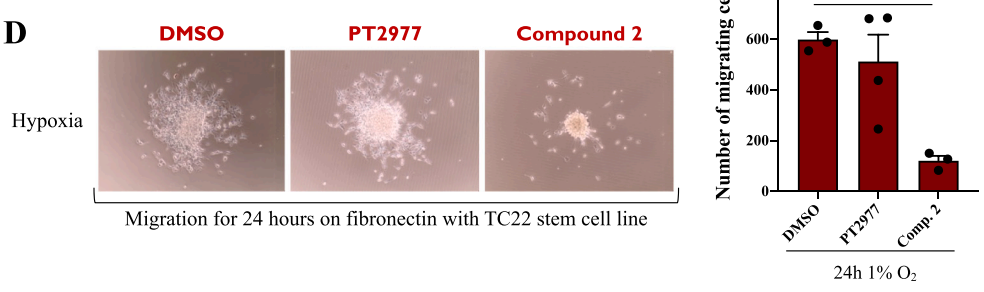

(caption on next page)

Fig. 6. Impact of hypoxia and ITGA5 on GSC proliferation and migration.
A – Neurosphere size as an index of stem cell proliferation (Incucyte) in normoxia (grey bars) or hypoxia (red bars for ITGA5 positive cells and blue bars for ITGA5 negative cells). The graphs represent the fold increase of neurosphere size at day 6 *versus* day of cell plating. B - Evaluation of inhibition of ITGA5 by a selective antagonist FR248, inhibition of HIF-2α by compound 2 inhibitor or both together on neurosphere size (Incucyte). C - Impact of ITGA5 expression on cell migration. Sphere formed for 48 h in methylcellulose were deposited either on poly-L-lysine or on fibronectin and treated or not with ITGA5 antagonist FR248 (20 μM) in normoxia or hypoxia. Histograms represent the number of cells migrating out of the TC22 spheres after 24 h either in normoxia or in hypoxia. D - Impact of the inhibition of HIF-2α on stem cell migration. Similar protocol as in B on fibronectin. PT2977 and compound 2 were applied at 20 μM. Data represent the mean ± S.E.M of 4 independent experiments with *p < 0.05; **p < 0.01; ***p < 0.005; ns = non-significant.

3.6. AHR expression is inversely correlated to HIF-2α and ITGA5 expressions in GSC

To be transcriptionally functional HIF-2α needs to heterodimerize with HIF1β/ARNT in the cell nucleus. ARNT (aryl hydrocarbon receptor nuclear translocator) also dimerizes with AHR (aryl hydrocarbon receptor). AHR plays complex roles in tumors including GBM [46] and has recently being described as a tumor suppressor-like gene in GBM whose repression induced migration and ITGA5 expression [47]. We wondered if AHR may affect the HIF-2α/ITGA5 axis in our models. AHR is strongly expressed in ITGA5 negative cell lines (NCH644, 5706, TC7) but less expressed in ITGA5 positive cells (3731, TC22) as shown by western blot (Fig. 7A) and immunocytochemistry (Fig. 7B). We wondered first if AHR antagonist (BAY218), which acts on the AHR cytoplasmic to nucleus translocation, may affect ITGA5 expression, but we did not observe any effect (data not shown). Following ligand binding, AHR protein is rapidly downregulated to regulate downstream signaling pathways [48]. We exploited this characteristic by subjecting TC22 and 3731 cells to the AHR agonist, compound 12a, during 72 h in hypoxia. In these conditions, AHR protein decreased drastically compared to control and concomitantly ITGA5 increased in both cell lines. Data suggest that HIF-2α and AHR expression levels are inversely linked to ITGA5 induction.

4. Discussion

Integrins are implicated in different hallmarks of cancer and particularly in GSC as reviewed recently [18,49–52]. Blocking their functions or inhibiting their expressions have been the subject of extensive preclinical studies with encouraging results. Clinical trials however failed to demonstrate integrin inhibitors efficacy in different solid tumors including GBM [53]. Among others, lack of knowledge on the heterogeneity of integrin expressions in patient's tumors may be involved in these clinical failures.

Concerning more particularly the ITGA5, its role in human cancer has been reviewed in [54]. Data confirm its role as a prognostic biomarker in solid tumors as for examples in laryngeal [55], head and neack [56], or oesophageal squamous cell carcinoma [57]. ITGA5 mediates tumor-stroma crosstalk to promote dissemination, metastasis and angiogenesis in liver, gastric, breast or pancreatic cancers [58–62]. In GBM, ITGA5 has been included in the mesenchymal subtype signature provided in the Verhaak classification [7]. Interestingly, its prognostic and therapeutic value has been confirmed in a recent publication which also demonstrated an impact of a high integrin expression on the tumor immune microenvironment [63]. Despite all the preclinical and clinical evidence that ITGA5 may be considered as a therapeutic target, clinical trials with Volociximab (a humanized anti-α5 antibody) failed [64]. We have shown previously that TMZ chemotherapy greatly affected the integrin repertoire in GBM differentiated cells [44] suggesting that anti-integrin therapies must be adjusted to the right patient but also to the right tumor progression time. In this work, we address more particularly the question of integrin expression in glioma stem cells submitted to hypoxia as experienced in hypoxic tumor niches.

To better understand the pattern of ITGA5 expression in GBM, we analyzed patient data and found that high integrin expressing tumors were correlated with exacerbated hypoxia pathway. Hypoxia is already known to maintain a GSC phenotype, to regulate their tumorigenic capacity and to initiate a mesenchymal switch [65–67]. We therefore focused on ITGA5 expression in GSC assuming that they are at the apex of tumor development and presumably at the origin of integrin expression heterogeneity. Our data confirm that not all GSC express ITGA5 and that hypoxia enhances it in selected cell lines. Results are in line with data showing a selective impact of hypoxia on the modulation of ITGA5 expression in breast cancer [68]. The hypoxic pathway is regulated by an induction of hypoxia-induced transcription factors, HIF-1α and HIF-2α. Both HIFs bind to a consensus HIF-binding site on the ITGA5 gene promoter in breast cancer cells and both are involved in ITGA5 mRNA and protein expression in these tumors [68]. However, HIF-2α plays specific oncogenic roles in tumors [69] and particularly in GBM where it appears as a key regulator in the hypoxic niche to maintain GSC stemness [70]. Our results are in line with HIF-2α controlling ECM-GSC interactions through modulation of ITGA5 expression and ITGA5-dependent cell migration. Targeting hypoxia became an interesting way to fight hypoxic tumors such as brain tumors and specific HIFs inhibitors were developed. We focused on HIF-2α selective inhibitors in our study: PT2977 and compound 2. This later molecule was one of the first small molecule designed in the field [42]. It binds only to the PAS-B domain (Per-ARNT-Sim-B) of HIF-2α thanks to the existence of a specific druggable pocket [42]. It prevents the HIF-2α/ARNT dimerization and transcription of HIF-2α target genes. PT2977 (Belzutifan) is a second-generation inhibitor that [41,71,72] was approved by the Food and Drug Administration (FDA) in 2021 for the treatment of Von Hippel-Lindau disease (VHL) in patients with renal cell carcinoma, central nervous system hemangioblastoma and pancreatic neuroendocrine tumors [73]. HIF-2α inhibitors were able to decrease ITGA5 expression and to inhibit GSC migration without affecting cell proliferation. Interestingly, combination of HIF-2α inhibitor with ITGA5 antagonist results in a strong anti-proliferative effect in hypoxia sensitive ITGA5 expressing cell lines. This new therapy combination may concern subclasses of GB patient tumors and particularly GSC in hypoxic niches and deserves further preclinical studies.

HIF-2α stabilization in hypoxia is however noted in all stem cell lines studied here even if levels of HIF-2α varied between different cell lines and do not always trigger ITGA5 expression. Other mechanisms of hypoxia-driven ITGA5 expression and functions have been highlighted recently. In head and neck squamous cell carcinoma, hypoxia increased tensin 4 which in turn stabilized integrin α5β1 complex [74]; In endothelial progenitor cells, hypoxia decreased ITGA5 but Nitric oxide restored ITGA5 through a miR-148/DNMT1 axis [75]. In this work we focused on a potential crosstalk between HIFs and AHR which has been highlighted recently. Both are members of bHLH-PAS family of transcription factors sharing similar DNA-binding motifs and heterodimerization with HIF1β/ARNT subunit. Although evidences suggest that HIF and AHR compete directly for binding to HIF1β/ARNT, interactions between associated transcription pathways appear more complex [76]. In cancers AHR is expressed in tumor cells but also in immune cells and AHR activation is linked to tumor progression and immunosuppression [77]. The role of AHR in tumors including GBM is however controversial with AHR activation related to bad prognostic [78–80] or AHR presumed to be a tumor suppressor [47,81]. AHR activation has been linked to integrin and matrix remodeling in different cell types and contexts [82]. As for example, AHR activation decreased ITGA6 integrin in breast cancer stem cells [83]. In our glioma stem cell models, AHR agonist-induced protein repression led to ITGA5 increase. Data confirm previous work in GBM cells where it was shown that AHR

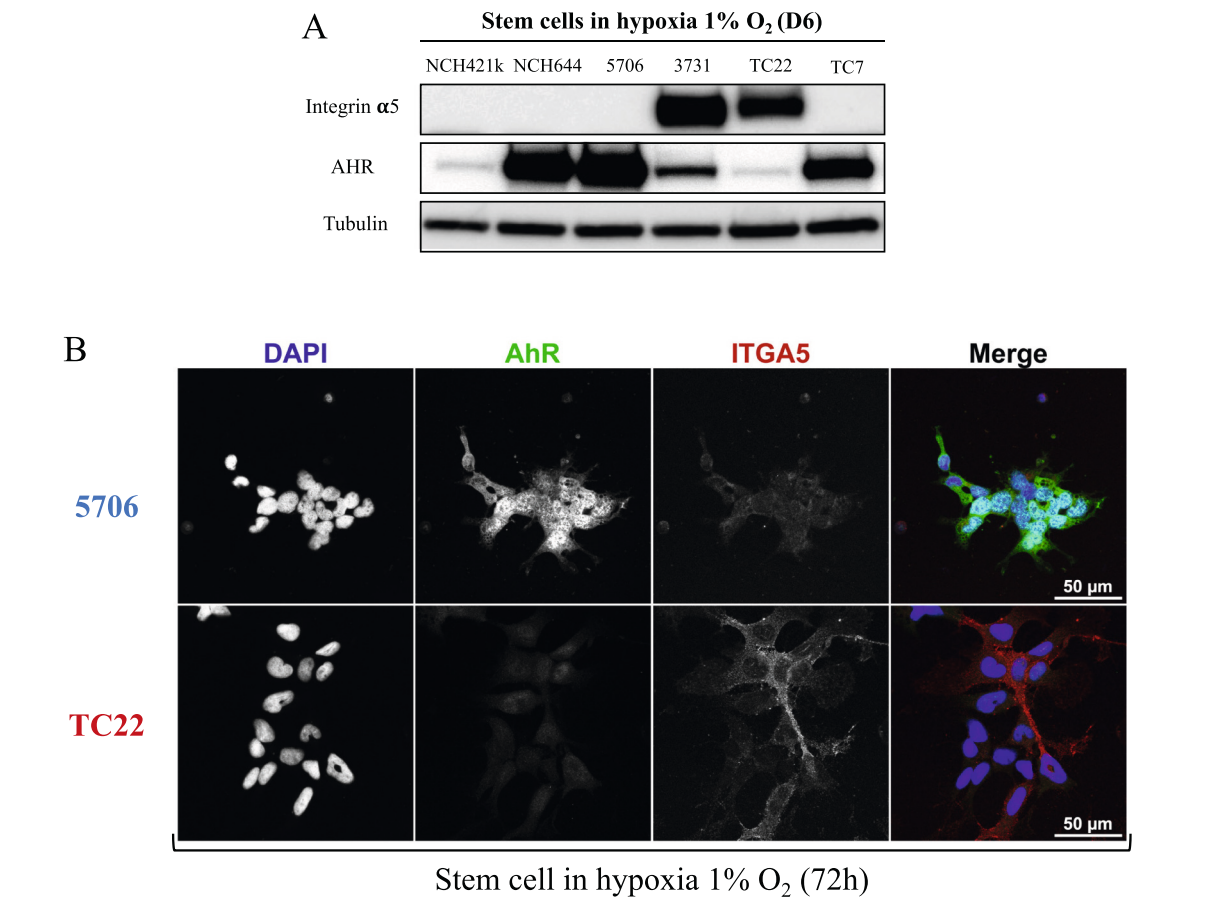

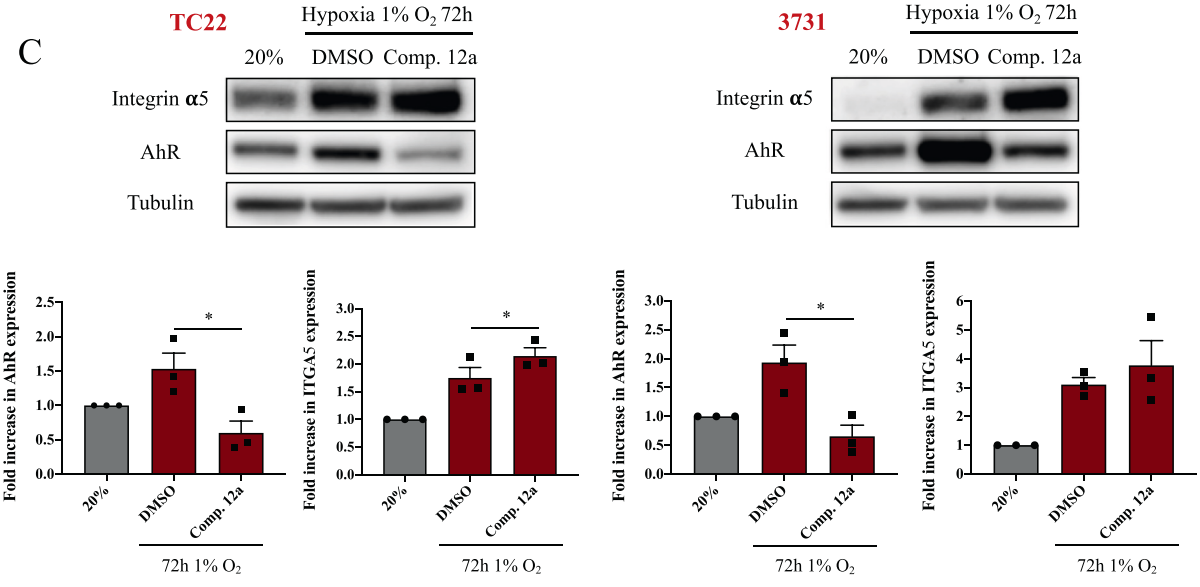

Fig. 7. Relationships between AHR, HIF-2α and ITGA5 expressions.
A - Western blot analysis of AHR and ITGA5 expressions in the 6 GSC lines after 6 days in hypoxia. B. Immunochemical staining of ITGA5 and AHR in 5706 GSC and TC22 GSC plated on polylysine and left 3 days in hypoxia. Nucleus staining with DAPI. C – TC22 and 3731 GSC were treated with an agonist of AHR (compound 12a - 20 µM) during 3 days in hypoxia and subjected to western blot analysis of AHR and ITGA5. Histograms represent the mean ± SEM of 3 independent experiments of the fold increase in proteins compared with the cells in normoxia.

silencing impact positively ITGA5 expression and cell migration [47]. Intriguingly AHR antagonist BAY218 did not affect AHR and ITGA5 expressions questioning the crosstalk of transcriptomic mechanisms between HIFs and AHR. According to our results we propose a new role of AHR as a modulator of protumoral targets, such as ITGA5, in some GSC and in specific conditions. Relationships between AHR and HIF-2α have to be finely characterized in the future and other molecular mechanisms involved in ITGA5 specific hypoxia-driven expression deserve further studies.

Notably, our study provides novel insight into one specific mechanism by which a GBM therapeutic target, the integrin ITGA5, may be differentially expressed in some glioma stem cells and modulated in specific tumor area. ITGA5 expression is also heterogeneous in more differentiated glioma tumor cells and in patient tumors revealing the complex modulation of this therapeutic target. As already demonstrated in differentiated GBM tumor cells, overexpression of this target confers migration advantages presumably implicated in brain dissemination of GSC cells. Targeting both HIF-2α and ITGA5 may be considered as a therapeutic option which deserves further studies in the future.

Funding

This project has received financial support from the CNRS through the 80|Prime program to support the PhD of Messe M., from Institut National du Cancer (INCA PLBIO 11527) and from ITI INNOVEC (IdEx (ANR-10-IDEX-0002), SFRI (ANR-20-SFRI-0012)).

CRediT authorship contribution statement

Mélissa Messé: Writing – review & editing, Writing – original draft, Methodology, Investigation, Formal analysis. **Chloé Bernhard:** Methodology, Investigation, Formal analysis. **Sophie Foppolo:** Methodology, Investigation. **Lionel Thomas:** Methodology, Investigation, Formal analysis. **Patrice Marchand:** Writing – review & editing, Methodology, Investigation, Data curation. **Christel Herold-Mende:** Resources. **Ahmed Idbaih:** Writing – review & editing, Resources. **Horst Kessler:** Resources. **Nelly Etienne-Selloum:** Methodology, Investigation, Formal analysis. **Charles Ochoa:** Resources. **Uttam K. Tambar:** Resources. **Mohamed Elati:** Formal analysis. **Patrice Laquerriere:** Writing – review & editing, Writing – original draft, Funding acquisition, Conceptualization. **Natacha Entz-Werle:** Writing – review & editing, Conceptualization, Writing – original draft. **Sophie Martin:** Writing – review & editing, Conceptualization, Writing – original draft. **Damien Reita:** Writing – review & editing, Writing – original draft, Visualization, Investigation, Formal analysis. **Monique Dontenwill:** Writing – review & editing, Writing – original draft, Supervision, Funding acquisition, Conceptualization, Methodology.

Declaration of competing interest

The authors declare that they have no known competing financial interests or personal relationships that could have appeared to influence the work reported in this paper.

Data availability

Data will be made available on request.

Acknowledgements

The experimental help of Bruno Jessel and the CYRCé platform.for PET experiences is highly acknowledged.

Appendix A. Supplementary data

Supplementary data to this article can be found online at https://doi.org/10.1016/j.bbadis.2024.167471.

References

[1] R. Stupp, W.P. Mason, M.J. van den Bent, et al., Radiotherapy plus concomitant and adjuvant temozolomide for glioblastoma, N. Engl. J. Med. 352 (2005) 987–996, https://doi.org/10.1056/NEJMoa043330.
[2] M.T. Ballo, P. Conlon, G. Lavy-Shahaf, et al., Association of Tumor Treating Fields (TTFields) therapy with survival in newly diagnosed glioblastoma: a systematic review and meta-analysis, J. Neuro-Oncol. 164 (2023) 1–9, https://doi.org/10.1007/s11060-023-04348-w.
[3] C.L. Nutt, D.R. Mani, R.A. Betensky, et al., Gene expression-based classification of malignant gliomas correlates better with survival than histological classification, Cancer Res. 63 (2003) 1602–1607.
[4] Cancer Genome Atlas Research Network, Comprehensive genomic characterization defines human glioblastoma genes and core pathways, Nature 455 (2008) 1061–1068, https://doi.org/10.1038/nature07385.
[5] C.W. Brennan, R.G.W. Verhaak, A. McKenna, et al., The somatic genomic landscape of glioblastoma, Cell 155 (2013) 462–477, https://doi.org/10.1016/j.cell.2013.09.034.
[6] H.S. Phillips, S. Kharbanda, R. Chen, et al., Molecular subclasses of high-grade glioma predict prognosis, delineate a pattern of disease progression, and resemble stages in neurogenesis, Cancer Cell 9 (2006) 157–173, https://doi.org/10.1016/j.ccr.2006.02.019.
[7] R.G.W. Verhaak, K.A. Hoadley, E. Purdom, et al., Integrated genomic analysis identifies clinically relevant subtypes of glioblastoma characterized by abnormalities in PDGFRA, IDH1, EGFR, and NF1, Cancer Cell 17 (2010) 98–110, https://doi.org/10.1016/j.ccr.2009.12.020.
[8] Q. Wang, B. Hu, X. Hu, et al., Tumor evolution of glioma-intrinsic gene expression subtypes associates with immunological changes in the microenvironment, Cancer Cell 32 (2017) 42–56.e6, https://doi.org/10.1016/j.ccell.2017.06.003.
[9] C. Neftel, J. Laffy, M.G. Filbin, et al., An integrative model of cellular states, plasticity, and genetics for glioblastoma, Cell 178 (2019) 835–849.e21, https://doi.org/10.1016/j.cell.2019.06.024.
[10] A.P. Patel, I. Tirosh, J.J. Trombetta, et al., Single-cell RNA-seq highlights intratumoral heterogeneity in primary glioblastoma, Science 344 (2014) 1396–1401, https://doi.org/10.1126/science.1254257.
[11] A. Dirkse, A. Golebiewska, T. Buder, et al., Stem cell-associated heterogeneity in glioblastoma results from intrinsic tumor plasticity shaped by the microenvironment, Nat. Commun. 10 (2019) 1787, https://doi.org/10.1038/s41467-019-09853-z.
[12] K. Mitchell, K. Troike, D.J. Silver, J.D. Lathia, The evolution of the cancer stem cell state in glioblastoma: emerging insights into the next generation of functional interactions, Neuro-Oncology 23 (2021) 199–213, https://doi.org/10.1093/neuonc/noaa259.
[13] J.A. Innes, A.S. Lowe, R. Fonseca, et al., Phenotyping clonal populations of glioma stem cell reveals a high degree of plasticity in response to changes of microenvironment, Lab. Investig. 102 (2022) 172–184, https://doi.org/10.1038/s41374-021-00695-2.
[14] M. Jackson, F. Hassiotou, A. Nowak, Glioblastoma stem-like cells: at the root of tumor recurrence and a therapeutic target, Carcinogenesis 36 (2015) 177–185, https://doi.org/10.1093/carcin/bgu243.
[15] K.P.L. Bhat, V. Balasubramaniyan, B. Vaillant, et al., Mesenchymal differentiation mediated by NF-κB promotes radiation resistance in glioblastoma, Cancer Cell 24 (2013) 331–346, https://doi.org/10.1016/j.ccr.2013.08.001.
[16] D. Stieber, A. Golebiewska, L. Evers, et al., Glioblastomas are composed of genetically divergent clones with distinct tumourigenic potential and variable stem cell-associated phenotypes, Acta Neuropathol. 127 (2014) 203–219, https://doi.org/10.1007/s00401-013-1196-4.
[17] A. Idbaih, Structural and functional intratumor heterogeneities in glioblastoma: a spacetime odyssey at single-cell level, Ann. Oncol. 28 (2017) 1415–1417, https://doi.org/10.1093/annonc/mdx217.
[18] A.-F. Blandin, F. Noulet, G. Renner, et al., Glioma cell dispersion is driven by α5 integrin-mediated cell-matrix and cell-cell interactions, Cancer Lett. 376 (2016) 328–338, https://doi.org/10.1016/j.canlet.2016.04.007.
[19] L. Seguin, J.S. Desgrosellier, S.M. Weis, D.A. Cheresh, Integrins and cancer: regulators of cancer stemness, metastasis, and drug resistance, Trends Cell Biol. 25 (2015) 234–240, https://doi.org/10.1016/j.tcb.2014.12.006.
[20] F. Schaffner, A.M. Ray, M. Dontenwill, Integrin α5β1, the fibronectin receptor, as a pertinent therapeutic target in solid tumors, Cancers (Basel) 5 (2013) 27–47, https://doi.org/10.3390/cancers5010027.
[21] L. Malric, S. Monferran, J. Gilhodes, et al., Interest of integrins targeting in glioblastoma according to tumor heterogeneity and cancer stem cell paradigm: an update, Oncotarget 8 (2017) 86947–86968, https://doi.org/10.18632/oncotarget.20372.
[22] J.D. Lathia, J. Gallagher, J.M. Heddleston, et al., Integrin alpha 6 regulates glioblastoma stem cells, Cell Stem Cell 6 (2010) 421–432, https://doi.org/10.1016/j.stem.2010.02.018.
[23] J.D. Lathia, M. Li, M. Sinyuk, et al., High-throughput flow cytometry screening reveals a role for junctional adhesion molecule a as a cancer stem cell maintenance factor, Cell Rep. 6 (2014) 117–129, https://doi.org/10.1016/j.celrep.2013.11.043.
[24] M. Nakada, E. Nambu, N. Furuyama, et al., Integrin α3 is overexpressed in glioma stem-like cells and promotes invasion, Br. J. Cancer 108 (2013) 2516–2524, https://doi.org/10.1038/bjc.2013.218.

[25] T.L. Haas, M.R. Sciuto, L. Brunetto, et al., Integrin α7 is a functional marker and potential therapeutic target in glioblastoma, Cell Stem Cell 21 (2017) 35–50.e9, https://doi.org/10.1016/j.stem.2017.04.009.
[26] P.A. Guerrero, J.H. Tchaicha, Z. Chen, et al., Glioblastoma stem cells exploit the αvβ8 integrin-TGFβ1 signaling axis to drive tumor initiation and progression, Oncogene 36 (2017) 6568–6580, https://doi.org/10.1038/onc.2017.248.
[27] L. Malric, S. Monferran, C. Delmas, et al., Inhibiting integrin β8 to differentiate and Radiosensitize glioblastoma-initiating cells, Mol. Cancer Res. 17 (2019) 384–397, https://doi.org/10.1158/1541-7786.MCR-18-0386.
[28] H. Janouskova, A. Maglott, D.Y. Leger, et al., Integrin α5β1 plays a critical role in resistance to temozolomide by interfering with the p53 pathway in high-grade glioma, Cancer Res. 72 (2012) 3463–3470, https://doi.org/10.1158/0008-5472.CAN-11-4199.
[29] R.S. Holmes, U.K. Rout, Comparative studies of vertebrate Beta integrin genes and proteins: ancient genes in vertebrate evolution, Biomolecules 1 (2011) 3–31, https://doi.org/10.3390/biom1010003.
[30] N. Etienne-Selloum, J. Prades, D. Bello-Roufai, et al., Expression analysis of α5 integrin subunit reveals its upregulation as a negative prognostic biomarker for glioblastoma, Pharmaceuticals (Basel) 14 (2021) 882, https://doi.org/10.3390/ph14090882.
[31] A. Subramanian, P. Tamayo, V.K. Mootha, et al., Gene set enrichment analysis: a knowledge-based approach for interpreting genome-wide expression profiles, Proc. Natl. Acad. Sci. USA 102 (2005) 15545–15550, https://doi.org/10.1073/pnas.0506580102.
[32] A. Liberzon, C. Birger, H. Thorvaldsdóttir, et al., The molecular signatures database (MSigDB) hallmark gene set collection, Cell Syst. 1 (2015) 417–425, https://doi.org/10.1016/j.cels.2015.12.004.
[33] E.C. Cosset, J. Godet, N. Entz-Werlé, et al., Involvement of the TGFβ pathway in the regulation of α5 β1 integrins by caveolin-1 in human glioblastoma, Int. J. Cancer 131 (2012) 601–611, https://doi.org/10.1002/ijc.26415.
[34] J.D. Lathia, J.M. Heddleston, M. Venere, J.N. Rich, Deadly teamwork: neural cancer stem cells and the tumor microenvironment, Cell Stem Cell 8 (2011) 482–485, https://doi.org/10.1016/j.stem.2011.04.013.
[35] S. Mohlin, A. Hamidian, K. von Stedingk, et al., PI3K-mTORC2 but not PI3K-mTORC1 regulates transcription of HIF2A/EPAS1 and vascularization in neuroblastoma, Cancer Res. 75 (2015) 4617–4628, https://doi.org/10.1158/0008-5472.CAN-15-0708.
[36] L. Holmquist-Mengelbier, E. Fredlund, T. Löfstedt, et al., Recruitment of HIF-1alpha and HIF-2alpha to common target genes is differentially regulated in neuroblastoma: HIF-2alpha promotes an aggressive phenotype, Cancer Cell 10 (2006) 413–423, https://doi.org/10.1016/j.ccr.2006.08.026.
[37] A. Pietras, D. Gisselsson, I. Ora, et al., High levels of HIF-2alpha highlight an immature neural crest-like neuroblastoma cell cohort located in a perivascular niche, J. Pathol. 214 (2008) 482–488, https://doi.org/10.1002/path.2304.
[38] S. Kummar, M. Raffeld, L. Juwara, et al., Multihistology, target-driven pilot trial of oral topotecan as an inhibitor of hypoxia-inducible factor-1α in advanced solid tumors, Clin. Cancer Res. 17 (2011) 5123–5131, https://doi.org/10.1158/1078-0432.CCR-11-0682.
[39] A. Nguyen, F.M. Moussalieh, A. Mackay, et al., Characterization of the transcriptional and metabolic responses of pediatric high grade gliomas to mTOR-HIF-1α axis inhibition, Oncotarget 8 (2017) 71597–71617, https://doi.org/10.18632/oncotarget.16500.
[40] E. Guérin, W. Raffelsberger, E. Pencreach, et al., In vivo topoisomerase I inhibition attenuates the expression of hypoxia-inducible factor 1α target genes and decreases tumor angiogenesis, Mol. Med. 18 (2012) 83–94, https://doi.org/10.2119/molmed.2011.00120.
[41] R. Xu, K. Wang, J.P. Rizzi, et al., 3-[(1S,2S,3R)-2,3-Difluoro-1-hydroxy-7-methylsulfonylindan-4-yl]oxy-5-fluorobenzonitrile (PT2977), a hypoxia-inducible factor 2α (HIF-2α) inhibitor for the treatment of clear cell renal cell carcinoma, J. Med. Chem. 62 (2019) 6876–6893, https://doi.org/10.1021/acs.jmedchem.9b00719.
[42] T.H. Scheuermann, Q. Li, H.-W. Ma, et al., Allosteric inhibition of hypoxia inducible factor-2 with small molecules, Nat. Chem. Biol. 9 (2013) 271–276, https://doi.org/10.1038/nchembio.1185.
[43] T.H. Scheuermann, D. Stroud, C.E. Sleet, et al., Isoform-selective and Stereoselective inhibition of hypoxia inducible Factor-2, J. Med. Chem. 58 (2015) 5930–5941, https://doi.org/10.1021/acs.jmedchem.5b00529.
[44] S. Sani, N. Pallaoro, M. Messe, et al., Temozolomide-acquired resistance is associated with modulation of the integrin repertoire in glioblastoma, impact of α5β1 integrin, Cancers (Basel) 14 (2022) 369, https://doi.org/10.3390/cancers14020369.
[45] G. Renner, F. Noulet, M.-C. Mercier, et al., Expression/activation of α5β1 integrin is linked to the β-catenin signaling pathway to drive migration in glioma cells, Oncotarget 7 (2016) 62194–62207, https://doi.org/10.18632/oncotarget.11552.
[46] T.X. Lim, M. Ahamed, D.C. Reutens, The aryl hydrocarbon receptor: a diagnostic and therapeutic target in glioma, Drug Discov. Today 27 (2022) 422–435, https://doi.org/10.1016/j.drudis.2021.09.021.
[47] U.-H. Jin, K. Karki, Y. Cheng, et al., The aryl hydrocarbon receptor is a tumor suppressor-like gene in glioblastoma, J. Biol. Chem. 294 (2019) 11342–11353, https://doi.org/10.1074/jbc.RA119.008882.
[48] R.S. Pollenz, The mechanism of AH receptor protein down-regulation (degradation) and its impact on AH receptor-mediated gene regulation, Chem. Biol. Interact. 141 (2002) 41–61, https://doi.org/10.1016/s0009-2797(02)00065-0.
[49] H. Hamidi, J. Ivaska, Every step of the way: integrins in cancer progression and metastasis, Nat. Rev. Cancer 18 (2018) 533–548, https://doi.org/10.1038/s41568-018-0038-z.
[50] C. Bergonzini, K. Kroese, A.J.M. Zweemer, E.H.J. Danen, Targeting integrins for cancer therapy - disappointments and opportunities, Front. Cell Dev. Biol. 10 (2022) 863850, https://doi.org/10.3389/fcell.2022.863850.
[51] D. Hanahan, Hallmarks of Cancer: new dimensions, Cancer Discov. 12 (2022) 31–46, https://doi.org/10.1158/2159-8290.CD-21-1059.
[52] M. Wang, S. Shen, F. Hou, Y. Yan, Pathophysiological roles of integrins in gliomas from the perspective of glioma stem cells, Front. Cell Dev. Biol. 10 (2022) 962481, https://doi.org/10.3389/fcell.2022.962481.
[53] E. Cruz Da Silva, M.-C. Mercier, N. Etienne-Selloum, et al., A systematic review of glioblastoma-targeted therapies in phases II, III, IV clinical trials, Cancers (Basel) 13 (2021) 1795, https://doi.org/10.3390/cancers13081795.
[54] J. Hou, D. Yan, Y. Liu, et al., The roles of integrin α5β1 in human Cancer, Onco Targets Ther 13 (2020) 13329–13344, https://doi.org/10.2147/OTT.S273803.
[55] C. Zhou, Y. Shen, Z. Wei, et al., ITGA5 is an independent prognostic biomarker and potential therapeutic target for laryngeal squamous cell carcinoma, J. Clin. Lab. Anal. 36 (2022) e24228, https://doi.org/10.1002/jcla.24228.
[56] B. Zou, D. Wang, K. Xu, et al., Integrin α-5 as a potential biomarker of head and neck squamous cell carcinoma, Oncol. Lett. 18 (2019) 4048–4055, https://doi.org/10.3892/ol.2019.10773.
[57] J.-J. Xie, J.-C. Guo, Z.-Y. Wu, et al., Integrin α5 promotes tumor progression and is an independent unfavorable prognostic factor in esophageal squamous cell carcinoma, Hum. Pathol. 48 (2016) 69–75, https://doi.org/10.1016/j.humpath.2015.09.029.
[58] S. Miyamoto, Y. Nagano, M. Miyazaki, et al., Integrin α5 mediates cancer cell-fibroblast adhesion and peritoneal dissemination of diffuse-type gastric carcinoma, Cancer Lett. 526 (2022) 335–345, https://doi.org/10.1016/j.canlet.2021.11.008.
[59] Z. Peng, M. Hao, H. Tong, et al., The interactions between integrin α5β1 of liver cancer cells and fibronectin of fibroblasts promote tumor growth and angiogenesis, Int. J. Biol. Sci. 18 (2022) 5019–5037, https://doi.org/10.7150/ijbs.72367.
[60] F. Pantano, M. Croset, K. Driouch, et al., Integrin alpha5 in human breast cancer is a mediator of bone metastasis and a therapeutic target for the treatment of osteolytic lesions, Oncogene 40 (2021) 1284–1299, https://doi.org/10.1038/s41388-020-01603-6.
[61] P.R. Kuninty, R. Bansal, S.W.L. De Geus, et al., ITGA5 inhibition in pancreatic stellate cells attenuates desmoplasia and potentiates efficacy of chemotherapy in pancreatic cancer, Sci. Adv. 5 (2019) eaax2770, https://doi.org/10.1126/sciadv.aax2770.
[62] T. Wang, J. Yang, J. Mao, et al., ITGA5 inhibition in pancreatic stellate cells re-educates the in vitro tumor-stromal crosstalk, Med. Oncol. 40 (2022) 39, https://doi.org/10.1007/s12032-022-01902-w.
[63] S. Li, N. Zhang, S. Liu, et al., ITGA5 is a novel oncogenic biomarker and correlates with tumor immune microenvironment in gliomas, Front. Oncol. 12 (2022) 844144, https://doi.org/10.3389/fonc.2022.844144.
[64] K.M. Bell-McGuinn, C.M. Matthews, S.N. Ho, et al., A phase II, single-arm study of the anti-α5β1 integrin antibody volociximab as monotherapy in patients with platinum-resistant advanced epithelial ovarian or primary peritoneal cancer, Gynecol. Oncol. 121 (2011) 273–279, https://doi.org/10.1016/j.ygyno.2010.12.362.
[65] Z. Li, S. Bao, Q. Wu, et al., Hypoxia-inducible factors regulate tumorigenic capacity of glioma stem cells, Cancer Cell 15 (2009) 501–513, https://doi.org/10.1016/j.ccr.2009.03.018.
[66] N.H. Boyd, A.N. Tran, J.D. Bernstock, et al., Glioma stem cells and their roles within the hypoxic tumor microenvironment, Theranostics 11 (2021) 665–683, https://doi.org/10.7150/thno.41692.
[67] L.A.D. Cooper, D.A. Gutman, C. Chisolm, et al., The tumor microenvironment strongly impacts master transcriptional regulators and gene expression class of glioblastoma, Am. J. Pathol. 180 (2012) 2108–2119, https://doi.org/10.1016/j.ajpath.2012.01.040.
[68] J.A. Ju, I. Godet, I.C. Ye, et al., Hypoxia selectively enhances integrin α5β1 receptor expression in breast Cancer to promote metastasis, Mol. Cancer Res. 15 (2017) 723–734, https://doi.org/10.1158/1541-7786.MCR-16-0338.
[69] A. Franovic, C.E. Holterman, J. Payette, S. Lee, Human cancers converge at the HIF-2alpha oncogenic axis, Proc. Natl. Acad. Sci. USA 106 (2009) 21306–21311, https://doi.org/10.1073/pnas.0906432106.
[70] S. Seidel, B.K. Garvalov, V. Wirta, et al., A hypoxic niche regulates glioblastoma stem cells through hypoxia inducible factor 2α, Brain 133 (2010) 983–995, https://doi.org/10.1093/brain/awq042.
[71] E. Jonasch, E.R. Plimack, T. Bauer, et al., 911PD - a first-in-human phase I/II trial of the oral HIF-2a inhibitor PT2977 in patients with advanced RCC, Ann. Oncol. 30 (2019) v361–v362, https://doi.org/10.1093/annonc/mdz249.010.
[72] W.W. Choi, J.L. Boland, A. Kalola, J. Lin, Belzutifan (MK-6482): biology and clinical development in solid tumors, Curr. Oncol. Rep. (2023), https://doi.org/10.1007/s11912-022-01354-5.
[73] E.D. Deeks, Belzutifan: first approval, Drugs 81 (2021) 1921–1927, https://doi.org/10.1007/s40265-021-01606-x.
[74] X. Zhao, Z. Mai, L. Liu, et al., Hypoxia-driven TNS4 fosters HNSCC tumorigenesis by stabilizing integrin α5β1 complex and triggering FAK-mediated Akt and TGFβ signaling pathways, Int. J. Biol. Sci. 20 (2024) 231–248, https://doi.org/10.7150/ijbs.86317.
[75] J. Behera, S. Govindan, M.S. Ramasamy, Nitric oxide promotes cell-matrix adhesion of endothelial progenitor cells under hypoxia condition via ITGA5 CpG promoter demethylation, Biochem. Biophys. Res. Commun. 644 (2023) 162–170, https://doi.org/10.1016/j.bbrc.2023.01.008.
[76] V.N. Lafleur, S. Halim, H. Choudhry, et al., Multi-level interaction between HIF and AHR transcriptional pathways in kidney carcinoma, Life Sci Alliance 6 (2023) e202201756, https://doi.org/10.26508/lsa.202201756.

[77] M.C. Takenaka, G. Gabriely, V. Rothhammer, et al., Control of tumor-associated macrophages and T cells in glioblastoma via AHR and CD39, Nat. Neurosci. 22 (2019) 729–740, https://doi.org/10.1038/s41593-019-0370-y.
[78] A. Sadik, L.F. Somarribas Patterson, S. Öztürk, et al., IL4I1 is a metabolic immune checkpoint that activates the AHR and promotes tumor progression, Cell 182 (2020) 1252–1270.e34, https://doi.org/10.1016/j.cell.2020.07.038.
[79] V. Panitz, S. Končarević, A. Sadik, et al., Tryptophan metabolism is inversely regulated in the tumor and blood of patients with glioblastoma, Theranostics 11 (2021) 9217–9233, https://doi.org/10.7150/thno.60679.
[80] D. Leclerc, A.C. Staats Pires, G.J. Guillemin, D. Gilot, Detrimental activation of AhR pathway in cancer: an overview of therapeutic strategies, Curr. Opin. Immunol. 70 (2021) 15–26, https://doi.org/10.1016/j.coi.2020.12.003.
[81] N. Mavingire, P. Campbell, T. Liu, et al., Aminoflavone upregulates putative tumor suppressor miR-125b-2-3p to inhibit luminal A breast cancer stem cell-like properties, Precis Clin. Med. 5 (2022) pbac008, https://doi.org/10.1093/pcmedi/pbac008.
[82] T. Kung, K.A. Murphy, L.A. White, The aryl hydrocarbon receptor (AhR) pathway as a regulatory pathway for cell adhesion and matrix metabolism, Biochem. Pharmacol. 77 (2009) 536–546, https://doi.org/10.1016/j.bcp.2008.09.031.
[83] E. Brantley, M.A. Callero, D.E. Berardi, et al., AhR ligand Aminoflavone inhibits α6-integrin expression and breast cancer sphere-initiating capacity, Cancer Lett. 376 (2016) 53–61, https://doi.org/10.1016/j.canlet.2016.03.025.